LBNL-40534
UC-405
Preprint

ERNEST ORLANDO LAWRENCE BERKELEY NATIONAL LABORATORY

Generalized Stability Analyses of Asymmetric Disturbances in One- and Two-Celled Vortices Maintained by Radial Flow

D. Nolan and B. Farrell

Computing Sciences Directorate
Mathematics Department

June 1997

Submitted to
Journal of the Atmospheric Sciences

REFERENCE COPY
Does Not
Circulate
Bldg. 50 Library - Ref.
Lawrence Berkeley National Laboratory
Copy 1
LBNL-40534

DISCLAIMER

This document was prepared as an account of work sponsored by the United States Government. While this document is believed to contain correct information, neither the United States Government nor any agency thereof, nor the Regents of the University of California, nor any of their employees, makes any warranty, express or implied, or assumes any legal responsibility for the accuracy, completeness, or usefulness of any information, apparatus, product, or process disclosed, or represents that its use would not infringe privately owned rights. Reference herein to any specific commercial product, process, or service by its trade name, trademark, manufacturer, or otherwise, does not necessarily constitute or imply its endorsement, recommendation, or favoring by the United States Government or any agency thereof, or the Regents of the University of California. The views and opinions of authors expressed herein do not necessarily state or reflect those of the United States Government or any agency thereof or the Regents of the University of California.

LBNL-40534

GENERALIZED STABILITY ANALYSES OF ASYMMETRIC DISTURBANCES IN ONE- AND TWO-CELLED VORTICES MAINTAINED BY RADIAL FLOW*

D. Nolan, and B. Farrell
Mathematics Department
Lawrence Berkeley National Laboratory
University of California
Berkeley, CA 94720

June 1997

* This report was prepared as part of the Ph.D. thesis of D. Nolan while a student at Harvard University, during which he was supported by the National Science Foundation Grant ATM-9216813 and National Science Foundation Grant 9623539; since November of 1996, D. Nolan has been supported by the U. S. Department of Energy under contract DE-AC03-76SF-00098. B. Farrell was supported by National Science Foundation Grant ATM-9216813 and National Science Foundation Grant 9623539.

Generalized Stability Analyses of Asymmetric Disturbances in One- and Two-celled Vortices Maintained by Radial Inflow

David S. Nolan[1]

Mathematics Group, Computing Sciences Directorate

Lawrence Berkeley National Laboratory

Berkeley, CA 94720

and

Brian F. Farrell

Department for Earth and Planetary Sciences

Harvard University

Cambridge, MA 02138

June, 1997

Submitted to ***Journal of the Atmospheric Sciences***

[1]Corresponding author address: 50A-2152, Lawrence Berkeley National Laboratory, 1 Cyclotron Road, Berkeley, CA 94720; *nolan@math.lbl.gov*

Abstract

We investigate the dynamics of both transient and exponentially growing disturbances in two-dimensional vortices that are maintained by the radial inflow of a fixed cylindrical deformation field. Such deformation fields are chosen so that both one-celled and two-celled vortices may be studied. We express the linearized evolution of asymmetric perturbations in the form of a linear dynamical system $d\mathbf{x}/dt = \mathbf{A}\mathbf{x}$. The shear of the mean flow results in a non-normal dynamical operator $\mathbf{A}$, allowing for the transient growth of perturbations even when all the modes of the operator are decaying. We find that one-celled vortices are stable to asymmetric perturbations of all azimuthal wavenumbers, while two-celled vortices can have low-wavenumber instabilities. In all cases, generalized stability analysis of the dynamical operator identifies the perturbations that grow the fastest, both instantaneously and over a finite period of time. While the unstable modal perturbations necessarily convert mean-flow vorticity to perturbation vorticity, the perturbations with the fastest instantaneous growth rate primarily rearrange their initial vorticity structures into higher-energy configurations. We also find perturbations that use a hybrid of these two mechanisms to achieve substantial energy growth over finite time periods.

We find that the radial inflow stabilizes the vortex in different ways for the two types of vortices considered. In one-celled vortex, the radial inflow suppresses transient growth for azimuthal wavenumbers by advecting perturbations out of the region of maximum shear and into the vortex core, thereby limiting the extent of the wave-mean flow interaction. In the two-celled vortex, it is found that elimination of the stretching and advection terms associated with the radial

inflow destabilizes the vortex for azimuthal wavenumbers one and two.

The effects of these perturbations on the mean flow through eddy flux divergences is also examined. In the one-celled vortex, it is found that for all wavenumbers greater than one, the net effect of most perturbations, regardless of their initial configuration, is to increase the kinetic energy of the mean flow. As these perturbations are sheared over they cause upgradient eddy momentum fluxes, thereby transferring their kinetic energy to the mean flow and intensifying the vortex. However, for wavenumber one in the one-celled vortex, and all wavenumbers in the two-celled vortex, we found that nearly all perturbations have the net effect of decreasing the kinetic energy of the mean flow. In these cases, the kinetic energy of the perturbations accumulates in nearly neutral or unstable modal structures, so that energy acquired from the mean flow is not returned to the mean flow but instead lost through dissipation.

1 Introduction

The role of asymmetry in primarily axisymmetric intense atmospheric vortices - such as waterspouts, tornadoes, and hurricanes - is the subject of this investigation. For waterspouts and tornadoes, these asymmetries include low-level windshear, the unsteady and asymmetric source of their angular momentum supply, and also the effects of turbulence. The success of recent three-dimensional numerical smulations in reproducing realistic maximum tornado windspeeds [Lewellen and Lewellen (1997)], compared with the much lower velocities predicted by theories and simulations based on axisymmetric models [Lilly (1969); Fiedler and Rotunno (1986); Fiedler (1994)], indicates that asymmetries may play an important role in the maintenance of an intense and robust tornadic vortex. For hurricanes, asymmetric forcing includes the beta effect, potential vorticity anomalies in the mid and upper levels of the atmosphere, and the shear of environmental winds; these asymmetries are believed to play a significant role in the track and intensity changes of these cyclones [Molinari (1992); Shapiro (1992); Montgomery and Farrell (1993); Smith and Weber (1993)].

The traditional approach to undertsanding the behavior of nearly axisymmetric vortices has relied heavily on straightforward stability analyses of their azimuthal velocity profiles, which in practice are approximated as a function of radius, either from measurements or from idealized functions (such as a Rankine vortex). A classical stability analysis is applied to small perturbations linearized about the mean azimuthal flow. If perturbations that grow exponentially in time

are found, the vortex is said to be unstable. Examples of this kind of analysis include those of Rotunno (1978), Staley and Gall (1979), Gall (1983, 1985), and more recently Steffens (1988), Flierl (1988), and Peng and Williams (1991). In accordance with traditional notions of stability in shear flows originally derived by Rayleigh (1880), most of these works found that a change in sign of the vorticity gradient of the azimuthal wind was necessary for the existence of instability. Additionally, some the analyses cited above also included the effects of a radially varying *vertical* wind which can create additional instabilities.

In recent years a new approach has been taken to the study of asymmetric dynamics in tropical cylcones which relies on the analysis of such perturbations as an initial-value problem rather than as an eigenvalue problem. Carr and Williams (1989) and Smith and Montgomery (1995) found linearized equations for the evolution of asymmetric disturbances in hurricane-like vortex flows, while Guinn and Schubert (1993) also included the results of numerical simulations of perturbed non-divergent barotropic flows in their analyses. The results of these studies show that asymmetric disturbances eventually decay rapidly with time due to the strong shear of the vortex, and that these decay rates increase with both the azimuthal and radial wavenumbers of the disturbances. Kallenbach and Montgomery (1995) also demonstrated how such disturbances can undergo a period of transient growth before decaying. However, their study was restricted to asymmetric initial conditions of arbitrary or convenient structure, and may have so far failed to identify the most important dynamics. Asymmetric dynamics have also been investigated by Willoughby (1992, 1995) for their role in determining tropical cylcone tracks, in regard to both the northwest drift of barotropic vortices due to the poleward increase of the coriolis parameter, and how these asymmetries can be used to determine the inital motion of the vortex in forecast models.

A simplifying assumption of great potential importance to the dynamics that was made in these stability studies of intense atmospheric vortices was neglecting the convergent background flow - the radial inflow - which forms and maintains these vortices. While initially this was justified by the belief that the radial velocities in the core of these vortices was negligible, it is now well known due to laboratory experiments [Wan and Chang (1972)], theoretical considerations [Burgraff, et. al. (1971)] and axisymmetric numerical simulations [Howells, et. al. (1985)] that there is in fact a strong radial inflow near the surface in tornadic vorticies, with velocities typically half as large as the azimuthal velocities. At some point as it approaches the central axis of the vortex, the radial inflow separates from the surface, turns upwards, and flows up and out of the vortex core. (Note: by the "core" of the vortex we mean inside, and in the vicinity of, the radius of maximum winds.) There is also substantial radial inflow in tropical cylcones, not only in the boundary layer, but also in the middle levels due to convective entrainment in the eyewall [Shapiro (1992)].

It is easy to imagine that this radial inflow may have important effects on the stability of these vortices. For example, one possible effect of this radial inflow could be to advect growing perturbations out of the region of maximum shear and inside the vortex core before it can grow substantially. In this sense, the radial inflow may render *all* growing perturbations "transient" by suppressing modal instability.

In this report we introduce a general method for determining the stability of two-dimensional vortex flows which includes the radial inflow that maintains the vortex. Furthermore, we will use an extension of the classical stability analysis, known as generalized stability analysis, to examine the growth of both transient and exponentially growing (if they exist) perturbations on the mean flow. Then we will examine specifically how these perturbations interact with the mean flow and the effects of radial inflow on the dynamics. In section 2 we will give an introduction to

generalized stability analysis; in section 3 we will describe our models of the idealized vortices under consideration; in section 4 we derive equations for the evolution of linearized asymmetric perturbations to these flows; in section 5 we will evaluate and comment on the stability of these vortices; in section 6 we will find the transient perturbations that grow the most in finite times; in section 7 we will investigate how these perturbations interact with the mean flow and how the presence of the radial inflow affects the results; and in section 8 we will discuss our conclusions.

2 Generalized Stability Theory

While the traditional approach to assessing the stability of observed flows in fluid dynamics and meteorology has been has been restricted to determining whether the flow supports exponentially growing modes, in recent years an alternative approach has developed. Inspired by the observation of Thompson (1887) and Orr (1907) that properly configured disturbances in stable shear flows undergo a finite period of energy growth before decaying, Farrell (1982) demonstrated the growth of baroclinic disturbances of this type in the atmospheric mid-latitude jet. The possibility of transient growth in the absence of exponentially growing modes is expressed mathematically by the fact that the non-normality of the linearized dynamical operator, i.e., that the dynamical operator does not commute with its transpose. Such transient growth may not be trivial: in Poiseuille flow at Reynolds number 5000, Butler and Farrell (1992) found disturbances that could grow in energy by a factor of 4897, despite the fact that Poiseuille flow is exponentially stable at this Reynolds number. This understanding has led to a general analysis of non-normal systems which has since been used extensively to understand transient growth in deformation and shear flows [Farrell (1988, 1989); Butler and Farrell (1992); Farrell and Ioannou (1993a, 1993b, 1996)]. Consideration of both transient and exponential growth processes has come to be called *generalized stability analysis*.

Let us describe in some detail how the non-normality of a system can lead to transient growth. First we write down the evolution of disturbances as a linear dynamical system:

$$\frac{d\mathbf{y}}{dt} = \mathbf{T}\mathbf{y} \tag{2.1}$$

where $\mathbf{y}$ is a function or vector that describes the state of the perturbation(s), and $\mathbf{T}$ is the time evolution operator. We also define a positive-definite Hermitian operator $\mathbf{M}$ such that the energy of the system can be written:

$$E = \mathbf{y}^*\mathbf{M}\mathbf{y} \tag{2.2}$$

We now perform the following useful change into *generalized velocity coordinates* $\mathbf{x}$:

$$\mathbf{x} = \mathbf{M}^{1/2}\mathbf{y} \tag{2.3}$$

$$\mathbf{A} = \mathbf{M}^{1/2}\mathbf{T}\mathbf{M}^{-1/2} \tag{2.4}$$

so that in generalized velocity coordinates:

$$\frac{d\mathbf{x}}{dt} = \mathbf{A}\mathbf{x} \tag{2.5}$$

$$E = \mathbf{x}^*\mathbf{x} \tag{2.6}$$

Equation (2.4) is a similarity transformation, so the eigenvalues of $\mathbf{A}$ are the same as the eigenvalues of $\mathbf{T}$. If all the eigenvalues of $\mathbf{T}$ have negative real part, then all the modes of $\mathbf{T}$ are decaying. So then are all the modes of $\mathbf{A}$, and we can conclude that the energy of the system goes to zero as $t \rightarrow \infty$. The structure in these generalized velocity coordinates that dominates energetically for large times will be the eigenvector of $\mathbf{A}$ associated with the eigenvalue with the largest real part, which we will call the *least damped mode*, or LDM. The structure of the LDM in the original coordinate system $\mathbf{y}$ can be found by transforming back into the orginal coordinates, i.e., inverting (2.3).

This does not address the issue of the energetics of the system at $t=0$ or for finite times. We can easily solve for the instantaneous rate of change in energy:

$$\frac{\partial E}{\partial t} = \frac{\partial}{\partial t}(\mathbf{x}^*\mathbf{x}) = \left(\frac{\partial}{\partial t}\mathbf{x}^*\right)\mathbf{x} + \mathbf{x}^*\left(\frac{\partial \mathbf{x}}{\partial t}\right) = \mathbf{x}^*\mathbf{A}^\dagger\mathbf{x} + \mathbf{x}^*\mathbf{A}\mathbf{x} = \mathbf{x}^*(\mathbf{A}^\dagger + \mathbf{A})\mathbf{x} \quad (2.7)$$

where the † refers to the Hermitian matrix transpose. Since the energy operator $(\mathbf{A}^\dagger + \mathbf{A})$ is normal and Hermitian, the eigenvector of $(\mathbf{A}^\dagger + \mathbf{A})$ with the largest eigenvalue will be at any instant the fastest growing (or least decaying) perturbation. This is certain because the eigenvectors of a normal matrix are complete and orthogonal - any other perturbation that does not project onto the dominant eigenvector could be constructed entirely from the other eigenvectors, all of which grow more slowly than the first. These perturbations are usually called the *instantaneous optimals* (IOs) of the system. By setting $\mathbf{x} = \mathbf{e}_{max}$ (the eigenvector with maximum eigenvalue) in equation (2.7), one can see that this upper bound on the normalized energy growth rate is:

$$\left(\frac{1}{E}\frac{\partial E}{\partial t}\right)_{max} = \lambda_{max} \quad (2.8)$$

where λ_{max} is the largest eigenvalue of $(\mathbf{A}^\dagger + \mathbf{A})$.

In regards to the issue of transient growth and non-normality, consider that when $\mathbf{A}$ is normal, $\mathbf{A}$ and $\mathbf{A}^\dagger$ have the same eigenvectors. Therefore the IO will be the same as the LDM, and its rate of change of energy will be twice the real part of the eigenvalue of the LDM. When $\mathbf{A}$ is non-normal, the eigenvalues and eigenvectors of $\mathbf{A}$ and the energy operator will be different, and any positive eigenvalues of the energy operator will correspond to transient growth as indicated by (2.8).

One can also find the perturbations of maximum growth over finite time, which we call *finite time optimals*, or FTOs. The energy as a function of time is:

$$E(t') = \mathbf{x}^*(t')\mathbf{x}(t') = \mathbf{x}^*(0)e^{\mathbf{A}^\dagger t'}e^{\mathbf{A}t'}\mathbf{x}(0) \tag{2.9}$$

Since the matrix product in (2.9) is normal and Hermitian, we see again that the eigenvector corresponding to the largest eigenvalue of $e^{\mathbf{A}^\dagger t}e^{\mathbf{A}t}$ will have the largest growth (or smallest decay) in energy between t=0 and t=t'. We have that:

$$\left(\frac{E(t')}{E(0)}\right)_{max} = \lambda_{max} \tag{2.10}$$

where here λ_{max} is the maximum eigenvalue of the matrix product $e^{\mathbf{A}^\dagger t}e^{\mathbf{A}t}$. Another approach to finding FTOs uses the singular value decomposition (SVD) of the propagator matrix $e^{\mathbf{A}t}$. The propagator matrix can be decomposed as:

$$e^{\mathbf{A}t} = \mathbf{UDV}^\dagger \tag{2.11}$$

where **U** and **V** are unitary matrices that can be interpreted to represent orthogonal decompositions of the domain and the range of the propagator, and **D** is a positive-definite diagonal matrix, the values of which represent the relative excitation of the system by their corresponding basis vectors. We can then write:

$$e^{\mathbf{A}^\dagger t}e^{\mathbf{A}t} = \mathbf{VDU}^\dagger\mathbf{UDV}^\dagger = \mathbf{VD}^2\mathbf{V}^\dagger \tag{2.12}$$

Clearly by previous argument the basis vector associated with the largest value of **D** will result in the most energy growth at time t, and the magnitude of the excitation will be the square of the largest element of **D**. The SVD approach is also be useful in that the maximal state of the FTO is produced in **U** simultaneously with its initial condition in **V**.

3 One-celled and Two-celled Vortices Maintained by Radial Inflow in a Closed Domain

As stated in the introduction we wish to investigate the dynamics of steady two-dimensional vortex flows that are generated when a cylindrical deformation field acts on a rotating fluid. In the following sections we will outline a method for finding such steady-state solutions given an arbitrary deformation field, and show how to choose such fields so as to produce either one-celled or two-celled vortices.

3.1 Formulation of the steady state solution in arbitrary deformation fields

The classic example of one such cylindrically symmetric flow is the well-known Burgers' vortex solution [Burgers (1948); also known as the Burgers'-Rott solution, see Rott (1958)]. Suppose that in an unbounded domain there exists a cylindrical deformation field of the form:

$$U = -\frac{1}{2}\alpha r \tag{3.1}$$

$$W = \alpha z \tag{3.2}$$

where U and W refer to the radial and vertical velocities in cylindrical coordinates. A steady state solution of the Navier-Stokes equations is obtained when the azimuthal velocity is:

$$V(r) = \frac{\Gamma_\infty}{2\pi r}(1 - e^{-\alpha r^2/4\nu}) \tag{3.3}$$

where Γ_∞ is the circulation at infinity, and ν is the kinematic viscosity. Note that this azimuthal velocity profile approaches solid body rotation for small r, and asymptotes to a potential vortex $(V = 1/r)$ for large r.

Suppose instead we assume an *arbitrary* cylindrical deformation field based on a radial inflow velocity field that is a function of r only:

$$U = U(r) \tag{3.4}$$

By continuity, we have:

$$\frac{\partial W}{\partial z} = -\frac{1}{r}\frac{\partial}{\partial r}(rU) \tag{3.5}$$

so that the vertical velocity field $W(r, z)$ may be determined up to constant. Holding the U and W velocities fixed, we can write down a single advection-diffusion equation for the evolution of the axisymmetric azimuthal velocity V:

$$\frac{\partial V}{\partial t} + U\frac{\partial V}{\partial r} + W\frac{\partial V}{\partial z} = \nu\left(\frac{\partial^2 V}{\partial r^2} + \frac{1}{r}\frac{\partial V}{\partial r} - \frac{V}{r^2}\right) \tag{3.6}$$

If the azimuthal velocity field is a function or r only, the vertical advection term may be neglected.

Now let us turn our attention to the solution of (3.6) in the finite domain $0 \le r \le b$, with boundary conditions $V(0) = 0$ and $V(b) = V_b$. We discretize V onto equally spaced gridpoints between $r=0$ and $r=b$, and write these values as the column vector **V**. Using matrix representations of standard finite difference operators, (3.6) may be represented as the inhomogeneous linear system:

$$\frac{\partial \mathbf{V}}{\partial t} = \mathbf{AV} + \mathbf{B} \tag{3.7}$$

where **B** is a column vector that allows us to incorporate the boundary conditions into the problem. Our steady state solution is found by solving for **V** such that its time derivative is zero:

$$\mathbf{V} = -\mathbf{A}^{-1}\mathbf{B} \tag{3.8}$$

Examples of some solutions of (3.8) are shown in the following sections.

3.2 One-celled vortices

While the Burgers' vortex solution is a useful point of reference, the fact that it resides in an unbounded domain creates serious difficulties for the analysis of asymmetric perturbations in

this flow. The greatest difficulties are those associated with the inflow of fluid through the edge of the domain at $r=b$. Let us instead create a deformation field similar to the Burgers' vortex deformation field, except that its support lies entirely within a cylinder of radius $r=b$; we will use $b=7$ for the rest of this work. Furthermore, we require that the radial inflow velocity transitions very smoothly to zero as we approach the outer boundary, and is nearly zero for a substantial region near the outer boundary. An example of such a radial inflow function is given by:

$$U(r) = -\alpha r e^{-\mu r^6} \tag{3.9}$$

This function with $\alpha = 5.0 \times 10^{-3}$ and $\mu = 2.44 \times 10^{-4}$ is shown in Figure 1a. This particular choice for α, in conjunction with a choice of $\nu=0.001$ for the viscosity, sets the radius of maximum winds $r_{max}=1$ for Burgers' vortex solution shown above. Using this radial velocity field and an outer boundary condition on V such that the circulation at the outer boundary $\Gamma_b = 2\pi r_b V_b = 2\pi$ (i.e., the circulation of the fluid at the edge of the domain is equal to 2π everywhere), (3.6) results in the solution shown in Figure 1b. This solution is virtually identical to the Burgers' solution with the same parameters, despite the fact that the radial inflow velocity transitions to zero near the outer edge of the domain. The deformation (or negative horizontal divergence) of the radial velocity function is shown in Figure 1c, while the radial gradient of the vertical vorticity is shown in Figure 1d.

3.3 Two-celled vortices

In light of observations, laboratory experiments, and both axisymmetric and three-dimensional numerical simulations, it is generally believed that many tornadoes (and other atmospheric vortices) have a stagnant core, in which air flows down from above along the center axis, diverges horizontally at the surface, and then recirculates upward along the annulus defined by the radius of maximum winds. Such a flow has come to be called a "two-celled" vortex. Perhaps the most

obvious example of a two-celled vortex in nature is the hurricane, which has a calm eye and generally descending motion inside the eyewall. We now present a simple model of such a vortex, by defining the radial velocity $U(r)$ to have inflow outside some radius, and outflow away from the r=0 axis, with a stagnation point in between:

$$U(r) = \begin{cases} 0 & r < 0.2 \\ 0.02\sin^2\left(\pi\frac{r-0.2}{1.6}\right) & 0.2 < r < 1 \\ 0.035\cos\left(\pi\frac{r-1}{2.0}\right) - 0.15 & 1 < r < 3 \\ -0.05\cos^2\left(\pi\frac{r-3}{7.0}\right) & 3 < r < 6.5 \\ 0 & r > 6.5 \end{cases} \tag{3.10}$$

This radial velocity function is shown in Figure 2a. Applying our method, where again we have defined the circulation at the outer boundary $\Gamma_b = 2\pi$, we find the azimuthal velocity profile shown in Figure 2b. The associated deformation function is shown in Figure 2c, while the resulting vertical vorticity gradient is shown in Figure 2d. We can see that outside the radius of maximum winds at r=2, the velocity profile is nearly exactly that of a potential flow, while inside the radius of maximum winds the velocity quickly drops to zero and the inner core is stangnant. The vorticity gradient changes sign in the *transition region* $1 < r < 2$, where the flow transitions from the potential flow to the inner stagnant core, indicating the possibility for instability as predicted by Rayleigh's (1880) theorem for growing disturbances in inviscid rotating flows.

4 The Evolution of Vertical Vorticity Perturbations in Idealized Vortices with Radial Inflow

4.1 Mathematical models of wave-mean flow interactions near and inside the vortex core

Investigations of atmospheric vortex dynamics face the problem of using finite resources

to investigate dynamics in an unbounded domain. Most work on vortex dynamics has used "solid wall" boundary conditions at some distance outside the vortex core to close the system [Howard and Gupta (1962); Staley and Gall (1979); Gall (1983); Staley and Gall (1984); Gall (1985); Steffens (1988); Peng and Williams (1991)]. This practice is analogous to the approximation of the midlatitude jet by bounded channel flows, and it is based on the reasonable assumption that disturbances to the mean flow that might lie outside of the "outer wall" will not unduly influence the results near or inside the vortex core. The results of such analsyses have generally been consistent with results derived from unbounded solutions based on semi-analytic methods such as contour dynamics [Rotunno (1978); Flierl (1988)], although Steffens (1988) did identify some significant changes in growth rates of a particular class of instabilities when the outer wall was moved farther away from the vortex core. While it might seem ideal to try instead to study the dynamics of localized perturbations in an unbounded vortex flow, Nolan (1996) found that having a mean flow in or out of the domain could result in spurious growth in energy of appropriately chosen initial perturbations. In that work, Nolan (1996) was able to eliminate the energy growth and other spurious results associated with having inflow through the boundaries, and other spurious results by placing, adjacent to the boundaries, regions of strong damping on the perturbation velocities.

In this work, however, we will return to the method of surrounding the dynamical region of interest (the vortex) with solid wall, free-slip boundaries. Furthermore, as described above in section 3, we have placed the same restrictions on the mean flow.

4.2 The linearized evolution of vertical vorticity perturbations

The specific vortex flows we will study have been outlined in section 3, but generally speaking we wish to describe the evolution of vertical vorticity perturbations in a swirling flow that has deformation and radial inflow that are functions of radius only. We restrict our attention to

the dynamics of the vertical vorticity component ζ, in cylindrical coordinates, where it assumed to have no variation in the vertical direction:

$$\frac{\partial\zeta}{\partial t}+u\frac{\partial\zeta}{\partial r}+\frac{v\partial\zeta}{r\partial\theta} = \zeta\frac{\partial w}{\partial z}+\nu\left[\frac{\partial^2\zeta}{\partial r}+\frac{1}{r}\frac{\partial\zeta}{\partial r}+\frac{1}{r^2}\frac{\partial^2\zeta}{\partial\theta}\right] \tag{4.1}$$

Now, we write each term in (4.1) as the sum of a radially varying mean and azimuthally, radially, and temporally varying perturbations: $u = U(r)+u'(r,\theta,t)$, $\zeta = Z(r)+\zeta'(r,\theta,t)$, and so on for v and w. Substituting these expressions into (4.1), we find the first order equation for the perturbations:

$$\frac{\partial}{\partial t}\zeta'+U\frac{\partial}{\partial r}\zeta'+\Omega\frac{\partial}{\partial\theta}\zeta'+u'\frac{\partial Z}{\partial r} = \zeta'\frac{\partial W}{\partial z}+\nu\left[\frac{\partial^2}{\partial r}+\frac{1}{r}\frac{\partial}{\partial r}+\frac{1}{r^2}\frac{\partial^2}{\partial\theta}\right]\zeta' \tag{4.2}$$

where we have written Ω for the mean angular velocity V/r. The last term on the left hand side represents the conversion of mean-flow vorticity to perturbation vorticity, which can result in instabilities.

Due to the azimuthal homogeneity of the background vortex, we can separate the solutions of (4.2) by writing them as a sum of harmonically varying azimuthal waves, i.e., $\zeta'(r,\theta,t) = \sum_k \zeta_k(r,t)e^{ik\theta}$, and so on for the perturbations of u and v also. Substituting these forms into (4.2), we create for each wavenumber k a linear equation for the evolution of the radially and temporally varying vorticity function $\zeta_k(r,t)$:

$$\left(\frac{\partial}{\partial t}+U(r)\frac{\partial}{\partial r}+ik\Omega(r)\right)\zeta_k+u_k\frac{\partial Z}{\partial r} = \zeta_k\frac{\partial W}{\partial z}+\nu\left[\frac{\partial^2\zeta_k}{\partial r^2}+\frac{1}{r}\frac{\partial\zeta_k}{\partial r}-\frac{k^2}{r^2}\zeta_k\right] \tag{4.3}$$

From here on we will use the convention that the terms u_k, v_k, ζ_k refer to complex amplitude

functions of r and t only.

4.3 The evaluation of velocities from the vorticity

As we can see from (4.3), when there is a non-zero background vorticity gradient, obtaining the evolution of the perturbation vorticity requires knowledge of the radial velocity perturbations. Furthermore, we anticipate the need to evaluate both u_k and v_k in the calculation of the perturbation kinetic energy and the eddy momentum fluxes. Following Carr and Williams (1989) and Smith and Montgomery (1995), we find the velocities by solving for the streamfunction:

$$\psi(r, \theta, t) = \sum_k \psi_k(r, t) e^{ik\theta} \tag{4.4}$$

$$u_k = \frac{-1}{r}\frac{\partial \psi_k}{\partial \theta} = \frac{-ik}{r}\psi_k \tag{4.5}$$

$$v_k = \frac{\partial \psi_k}{\partial r} \tag{4.6}$$

$$\zeta_k = \frac{1}{r}\left[\frac{\partial}{\partial r}(r v_k) - \frac{\partial u_k}{\partial \theta}\right] = \left[\frac{\partial^2}{\partial r^2} + \frac{1}{r}\frac{\partial}{\partial r} - \frac{k^2}{r^2}\right]\psi_k \tag{4.7}$$

As previously discussed, we choose the boundary conditions of no normal flow at the outer boundary $r=b$, i.e.:

$$\psi_k(0, t) = \psi_k(b, t) = 0 \tag{4.8}$$

Given the vorticity, in the case of continuous functions equation (4.7) may be inverted with a Green's function:

$$\psi_k(r, t) = \int_a^b G_k(r, \rho)\zeta_k(\rho, t) d\rho \tag{4.9}$$

The Green's function appropriate for this problem is [from Carr and Williams (1989), with the inner boundary a set to zero]:

$$G_k(r,\rho) = \begin{cases} \dfrac{r^{2k}}{2kr^k b^{2k}}(\rho^{k+1} - b^{2k}\rho^{-k+1}) & 0 \le r \le \rho \\ \dfrac{r^{2k} - b^{2k}}{2kr^k b^{2k}}\rho^{k+1} & \rho \le r \le b \end{cases} \tag{4.10}$$

which can be found using standard techniques [Case (1960)].

4.4 The solution and analysis of the system

We would like to express the evolution of the perturbations as a linear dynamical system. We discretize the domain by assigning the values of the radial functions to evenly spaced points from $r = 0 + \Delta r$ to $r = b - \Delta r$, each point separated by a distance Δr. This converts the continuous radial functions into vectors of length $N = (b/\Delta r) - 1$. We express all derivatives as matrix operators corresponding to the usual centered-difference approximations, with the exception that the finite difference operator used for the advection term is one-sided so that it represents a second-order upwinding advection scheme. We must also express the Green's function operation (4.9) as a matrix operation, i.e.:

$$\psi_k = \mathbf{G}_k \zeta_k \tag{4.11}$$

where k refers to the wavenumber, and the operator $\mathbf{G}_k$ is defined as above according to (4.9). Once the Green's function and finite difference operators are defined, one can easily combine them to produce the desired information from the source vorticity vectors. For example, from (4.5) we would have:

$$u_k = -ik\mathbf{R}^{-1}\mathbf{G}_k\zeta_k \tag{4.12}$$

Operators that refer to functions of r only, such as the $\mathbf{R}^{-1}$ operator, are simply diagonal matrices with the function values on the diagonal.

Finally, we take vorticity evolution equation (4.3) and manipulate it into a form with only the time derivative on the L.H.S., and install the matrix operators accordingly. The result is:

$$\frac{d\zeta_k}{dt} = \mathbf{T}_k \zeta_k \tag{4.13}$$

with:

$$\mathbf{T}_k = -\mathbf{U}\mathbf{D}_{up} - ik\Omega + (\mathbf{D}\mathbf{Z})ik\mathbf{R}^{-1}\mathbf{G}_k + \mathbf{S} + \nu(\mathbf{D}^2 + \mathbf{R}^{-1}\mathbf{D} - k^2\mathbf{R}^{-2}) \tag{4.14}$$

Where we have written $\mathbf{D}$ for the matrix representing the finite-difference calculation for the derivative with respect to r, $\mathbf{D}_{up}$ for a similar but upwinded deriviative operator, and $\mathbf{S}$ for the "stretching" term $\partial W/\partial z$. We must also incorporate into these difference operators additional boundary conditions on the vorticity, which we choose to be:

$$\zeta_k(0) = \zeta_k(b) = 0 \tag{4.15}$$

This condition prevents the advection and diffusion of perturbation vorticity into the domain from the boundaries. The solution of (4.13) in time is:

$$\zeta_k(t) = e^{\mathbf{T}_k t}\zeta_k(0) \tag{4.16}$$

4.5 The kinetic energy of the perturbations

The kinetic energy for each perturbation in continuous space is:

$$E = \int_0^b \left(\frac{\overline{u_k^2}}{2} + \frac{\overline{v_k^2}}{2} \right) 2\pi r dr \tag{4.17}$$

where the overbars refer to averages around the azimuth of the real parts of the complex velocity functions. A streamfunction-vorticity formulation for the energy can be found by using (4.5)-(4.9) and integrating by parts to find:

$$E = -\frac{1}{2}\int_0^b \overline{\psi_k \zeta_k} 2\pi r dr \tag{4.18}$$

Using the fact that $\overline{pq} = \frac{1}{4}(p^*q + q^*p)$ we can re-write (4.18) as:

$$E = -\frac{\pi}{4}\int_0^b (\psi_k{}^*\zeta_k + \zeta_k{}^*\psi_k) r dr \tag{4.19}$$

As discussed in section 2 it is useful to find an energy metric operator **M** such that the energy of our discretized linear dynamical system may be written $E = \zeta^*\mathbf{M}\zeta$. For each azimuthal wavenumber k the energy metric can be formulated from (4.19):

$$\mathbf{M}_k = \frac{-\pi\Delta r}{4}[\mathbf{G}_k{}^\dagger\mathbf{R} + \mathbf{R}\mathbf{G}_k] \tag{4.20}$$

5 Stability

5.1 The stability of the one-celled vortex

Now let us focus our attention on the one-celled vortex as described in section 3.2. The nearly identical Burgers' vortex solution has been previously found to be stable to all two-dimensional disturbances by Robinson and Saffman (1984); however, their analysis relied on a low-Reynolds number expansion, which clearly has limited application to atmopsheric vortices or to our one-celled vortex with ν=0.001. Figure 3 shows the real part of the eigenvalue of the LDM for each azimuthal wavenumber from k=1 to k=12. We can see that for these wavenumbers the one-celled vortex is asymptotically stable and the trend of the plot suggests that no unstable modes exist for any azimuthal wavenumber. The decay rate of these modes is clearly linear with respect to azimuthal wavenumber, with the exception that the k=1 decay rate appears exceptionally smaller than the trend of the the other LDM decay rates would indicate. The linearity of the decay rate is indicative that it is the interaction with the shear of the swirling flow, rather than diffusion, that contributes the most to the decline of the amplitudes of these modes.

Figure 4 shows vorticity and streamfunction contour plots of the LDM for the first two azi-

muthal wavenumbers. These two modes are considerably different. For k=1, the LDM is a dipole-like structure whose vorticity lies entirely inside the core of the vortex. For k=2, the LDM lies at the outer edge of the domain and spirals inward in the same direction as the mean flow. In fact, the LDMs for all higher wavenumbers are higher-wavenumber replicas of the k=2 LDM.

Why is the k=1 LDM distinct from those of all higher wavenumbers? There are two reasons. Firstly, k=1 perturbations experience considerably less disspiation near r=0 than higher wavenumber perturbations - this is due to the $-k^2/r^2$ term in the diffusive part of (4.3). Secondly, the perturbation velocities do not go to zero at r=0, which is to say that only for k=1 can there be perturbation flow across the r=0 axis. In the case of the one-celled vortex, this allows the k=1 LDM to convert more mean-flow vorticity to perturbation vorticity, thereby helping to sustain itself. It is for this reason that the decay rate of the k=1 LDM is so small. Since the higher wavenumber perturbations are therefore generally not well suited to persist in the core of the vortex, their LDMs lie instead as far away from the core as posible so that they are subjected to as little diffusion and deformation as possible. For this reason, the structures and locations of the LDMs for k=2 and higher are entirely dependent on the location of the outer boundary of the domain. Fortunately, we shall see that only these important modes - the LDMs for k>1 in the one-celled vortex - suffer this defect.

5.2 The stability of the two-celled vortex

We turn our analysis now to the two-celled vortex described in section 3.3. Figure 5 shows the real parts of the eigenvalues of the LDMs for azimuthal wavenumber k=1 through k=15. We can see that there is a window of instability from k=3 to k=10. This result is a 'classic' curve which has been produced in many previous studies of the stability of rotating flows, particularly Staley and Gall (1979), Gall (1985), Steffens (1988), and Peng and Williams (1991). Our curve is

slightly different from these earlier results due to the presence of dissipation, so that the stable modes are not neutral but rather have negative growth rates which bring the curve in Figure 5 below the horizontal axis outside the unstable wavenumber range.

The vorticity and streamfunction fields for the most unstable (least damped) mode for the first azimuthal wavenumber with instability, k=3, and the most unstable wavenumber, k=5, are shown in Figure 6. These modes are quite similar in structure, consisting of two concentric rings of ellipse-shaped vorticity perturbations, alternating in sign, located in the transition region between r=1 and r=2, with the two rings of perturbations shifted in phase from each other such that the inner rings lead the outer rings by almost exactly half a cycle. These modes operate with a mechanism that is the same as the two-dimensional modes identified in the earlier vortex stability studies noted above - see in particular Staley and Gall (1979), Gall (1983), and Flierl (1988). That is to say, they persist and/or grow through the familiar mechanism of converting mean flow vorticity to perturbation vorticity via the $u_k(\partial Z/\partial r)$ term in (4.3). In Figure 7, the modes show another common aspect of classical instabilities in that the angular velocity (phase speed) of the unstable modes is representative of the local mean flow angular velocity, while the decaying modes have a much lower angular velocity, indicating they are rapidly retrograding against the mean flow. The maximum angular velocity V/r in the two celled vortex is Ω=0.23, while halfway through the transition region the angular velocity is Ω=0.15, which compares very favorably with the phase speeds of the unstable modes.

6 Optimal Growth Perturbations

As Orr (1907) originally observed, the growth of a perturbation in linear, inviscid shear flow is determined solely by how far back against the shear the disturbance is originally tilted. A

perturbation whose phase lines are tilted all the way back becoming nearly parallel with the flow could conceivably have unlimited growth. In more realistic flows this is prevented by diffusion. With this in mind, it is easy to imagine that the perturbation that would grow the most in an asymptotically stable inviscid vortex without radial inflow would be a vorticity perturbation that spirals back against the flow at an angle such that azimuthal advection would uncoil the vorticity of the perturbation, reducing its radial wavenumber until the vorticity contours were radially aligned at the moment of maximum perturbation amplitude. Viscosity would limit the possible maximum growth of such a perturbation: the tighter the spiral (in either direction) made by the perturbation, the faster viscosity would diffuse the vorticity.

The structures of IOs are usually quite different. The IOs seek out the part of the flow which has the most shear or deformation, and arrange the vorticity there to create the fastest possible instantaneous growth in perturbation energy. This is usually a structure that locally tilts back against the shear of the flow at an angle of 45 degrees, a geometry which maximizes the eddy fluxes $\overline{u'v'}$, and at the same time places the perturbation in the orientation leading to maximum rate of decrease in wavenumber from advection by the local difluent component of the shearing velocity field.

We now turn our attention to such transient growing modes which can be identified with the procedures and analysis outlined in section 2. We will show that even for the wavenumbers for which the vortex is asymptotically stable there can be significant transient perturbation growth.

6.1 Instantaneous and finite-time optimals in the one-celled vortex

Figure 8 shows the vorticity and streamfunction fields for the k=1 and k=2 IOs on our one-celled vortex. We can see these perturbations have structures very much like those predicted above: the vorticity contours spiral back against the shear of the mean flow. The streamfunction

contours show that the perturbation velocities flow back against the shear of the vortex at the expected angle of 45 degrees which maximizes the eddy fluxes, and the place where this occurs is in the vicinity of r=1, where the maximum shear exists (note that in a vortex, the "shear" is not the rate of change of velocity but rather the rate of change of angular velocity). The k=2 IO is essentially a higher-waveumber replica of the k=1 IO, and this was found to be true for all wavenumbers. The normalized IO growth rates for k=1 through k=12 is shown in Figure 9. The growth rate increases from 0.4 at k=1 to 0.55 at k=4 and then quickly decreases. While in inviscid flows, such growth rates are known to increase asymptotically with wavenumber towards a limit determined by the maxmimum deformation of the mean flow [Howard (1972)], the decline after k=4 in our vortex is caused by the increasing effects of viscosity on higher-wavenumber structures.

Figure 10a-b show the vorticity and streamfunction for the k=1 FTO for a transient growth time of t=8.98. This corresponds to the time it takes for the mean flow to travel one circuit around the vortex at r=1. We again see the expected result that the perturbation spirals back against the mean flow, and it does so almost exactly once. We also note, however, that the vorticity of the FTO lies not in the immediate vicinity of r=1 but rather at a small distance outside of r=1. This displacement is indicative of the effect of radial inflow: as the vorticity is uncoiled it is also carried inwards towards r=1. Figure 10c-d show the structure of this perturbation when it has reached its maximum energy at t=8.98; we call this structure the *realized finite time optimal*, or RFTO, and obtain it from the SVD of the propagator as outlined in section 2. This confirms the hypothesis that the perturbation reaches is maximum energy when the vorticity contours have been completely uncoiled, and it also shows that the radial inflow has carried the vorticity into the core of the vortex during this process.

Figure 11 shows the maximum transient growth in energy as a function of time for k=1

and k=2 perturbations in the one-celled vortex. For k=1, the maximum possible normalized energy growth is a factor of 181, which occurs at the time of t=131; the perturbation that realizes this growth is called the *global optimal* (GO), and its maximal state will be called the *realized global optimal* (RGO). We see that the potential for transient growth of k=2 perturbations is substantially less than that of k=1 perturbations, with a maximum potential growth factor of only 33 occurring at t=17. The GO for k=1, and it's realization, are shown in Figure 12. The GO is a structure whose vorticity spirals far back against the mean flow, and it lies in the vicinity of r=5, which is the farthest extent of the field of substantial inflow velocities (see Figure 1a), while the RGO shows again that this perturbation reaches its maximum energy when its vorticity has been advected into a dipole-like structure in the core of the vortex.

6.2 IOs and FTOs in the two-celled vortex: the stable regime

As we saw above, the two-celled vortex we have generated is stable for azimuthal wavenumbers k=1, k=2, and k>10. Thus we can expect that wave-mean flow interactions at these stable wavenumbers will be dominated by the optimal transients. Figure 13 shows the IOs for k=1 and k=2. The vorticities of these perturbations are again arranged to create down-gradient eddy fluxes at the location of the maximum shear in the mean flow, which lies in the center of the transition zone between the exterior potential flow and the stagnant interior. Figure 14 shows the IO growth rates for azimuthal wavenumbers k=1 through k=15. Comparison with Figure 5 indicates that the transient optimals can grow faster than their corresponding LDMs for all wavenumbers, even when unstable modes are present.

Figure 15 shows the maximum transient growth as a function of time for k=1 and k=2 in the two-celled vortex. While the growth in energy by a factor of 94 for k=1 is substantial, the growth by a factor of 2886 for k=2 is tremendous. The initial and maximal states of the k=2 GO

can be seen in Figure 16. The initial state is the familiar reverse spiral, also displaced outward from the vortex core, like those we saw for the one-celled vortex. The maximal state, however, is considerably different than those we saw in the one-celled vortex. Rather than forming into a coherent quadropole structure (which we might expect for the maximal state of a wavenumber two optimal), the GO evolves into a structure whose vorticity field is a lower-wavenumber version of the unstable modes (see Figure 6). Why does this occur? As the GO is deformed and advected into the vortex core, it ineracts with the vorticity gradient of the mean flow. As it does so, it converts mean-flow vorticity into perturbation vorticity, thereby modifying the structure it would have if the only effect of the mean flow were deformation of the perturbation vorticity field. While *any* initial perturbation in *any* linearized system will indeed be dominated by the LDM in the limit as $t \to \infty$, the reason that we find such large transient growth for low wavenumbers in the two-celled vortex is that the energy acquired from the mean flow via the Orr mechanism accumulates in these very persistent LDMs, rather than being returned to the mean flow as the perturbation is sheared over.

6.3 Transient and long-term growth in the unstable regime

Are transient growth processes relevant in the unstable regime? Since the eigenvectors of $\mathbf{T}_k$ (for each particular wavenumber k) are not orthogonal to each other, an arbitrary perturbation will almost surely project to some extent onto the most unstable mode, thereby exciting an exponentially growing perturbation. The total perturbation will then be asymptotically dominated by the unstable LDM. For linear systems with normal dynamical operators, the initial condition that achieves the greatest long-term growth would not surprisingly be the LDM itself. It is interesting to note, however, in non-normal systems such as these vortex/shear flows, the perturbation that excites the LDM the most for all times is not the LDM itself, but rather the LDM of the adjoint

operator $\mathbf{A}^\dagger$ (hereafter referred to as the LDMA). This was remarked by Farrell (1988) for neutral Rossby waves, but the argument is general and has been further discussed by Farrell and Ioannou (1996).

To see this mathematically, first recall that the solution in time to our linear dynamical system in generalized velocity coordinates (2.5) is:

$$x(t) = e^{\mathbf{A}t}x(0) \tag{6.1}$$

Now consider the following standard diagonalization of the propagator matrix:

$$e^{\mathbf{A}t} = \mathbf{E}e^{\mathbf{D}t}\mathbf{E}^{-1} \tag{6.2}$$

where $\mathbf{D}$ is a diagonal matrix with the eigenvalues of $\mathbf{A}$ on its diagonal and $\mathbf{E}$ is a matrix whose columns are the eigenvectors of $\mathbf{A}$. We may assume that the eigenvalues and eigenvectors are ordered such that the LDM lies in the first column of $\mathbf{E}$ and its eigenvalue is the first element of $\mathbf{D}$. For large times the resultant propagator matrix is dominated by the contribution of the the dominant eigenmode, the LDM. Therefore:

$$\lim_{t \to \infty} e_{kl}^{\mathbf{A}t} = \mathbf{E}_{k1}e^{\mathbf{D}_{11}t}\mathbf{E}_{1l}^{-1} \tag{6.3}$$

The dominance of the LDM is indicated by the fact that it is the only one of the eigenvectors of $\mathbf{A}$ that appears in this limit. What initial condition maximizes (in a normalized sense) the response of the LDM for large times? It is the one that maximizes its inner product with the rightmost term of (6.3). By Schwarz's inequality and our definition of the energy norm (2.6), this is the complex conjugate of the rightmost term, i.e., $(\mathbf{E}_{1l}^{-1})^*$. Finally, since the diagonalization of the *adjoint* propagator is:

$$e^{\mathbf{A}^\dagger t} = (\mathbf{E}^{-1})^\dagger e^{\mathbf{D}^\dagger t}\mathbf{E}^\dagger \tag{6.4}$$

we observe that our desired initial condition is identical to the LDM of the adjoint of the dynamical operator **A**.

Figure 17 shows the logarithm of the energy as a function of time for three k=3 perturbations on the two-celled vortex: the LDM, the LDMA, and the t=5 FTO. The LDM undergoes a steady exponential growth rate from t=0 onward. The LDMA grows in energy even more rapidly than the LDM for a finite period of time, and then settles into the same exponential growth rate, but with 4.04 times as much energy at later times than the LDM. The FTO has an even faster initial growth rate, but after longer times has less energy than the LDMA. Examination of the LDMA and FTO vorticity and streamfunction fields, as shown in Figure 18, is revealing. These structures are similar to the LDM in the vortex core, but outside of r=2 they have the familiar reverse spiral. Thus we can see that their "extra" energy growth for short times comes from the transient growth associated with the uncoiling of the reverse spirals. We note that all the FTOs for growth times t>20 (not shown) were identical to the LDMA. While for long times the structures which will dominate the perturbations for the unstable wavenumbers are indeed the unstable LDMs, the initial condition that leads the most rapid appearance of the LDM is in fact the LDMA.

7 Analysis

In this section we will examine two issues not directly addressed by the identification of the least damped modes and/or the transiently growing optimals. The first issue will concern the exchange of energy between the perturbations and the mean flow, and the second issue will be the effect on the results of the presence of the cylindrical deformation fields, i.e., the radial inflow.

7.1 Wave-mean flow interactions

Energy is exchanged between the mean flow and the perturbations via eddy fluxes. These eddy fluxes affect the mean flow through the divergence of the volume-averaged eddy flux terms

previously neglected in the mean flow equations such as (3.6). The change to the mean azimuthal velocity caused by the perturbation eddy flux divergences is [Carr and Williams (1989); Montgomery and Kallenbach (1995)]:

$$\frac{\partial V}{\partial t} = -\frac{1}{r^2}\frac{\partial}{\partial r}\overline{(r^2 u'v')} = -\overline{u'\zeta'} \tag{7.1}$$

where the overbars refer to azimuthal averages and the primes refer to the perturbation velocities and vorticities. These terms can be easily calculated to indicate - in the linear limit where we assume that the actual change of the mean flow is negligible - where the mean flow energy exchange is taking place and how the mean flow would indeed be changed if the perturbations were of substantial amplitude. The perturbations themselves, being asymmetric, have zero net momentum. They change the kinetic energy of the mean flow by rearranging its momentum via eddy momentum fluxes. Upgradient (downgradient) momentum fluxes cause an increase (decrease) in mean flow kinetic energy. This can be seen from examination of two forms of the equation for the rate of change of perturbation kinetic energy for the case we are studying: strictly two-dimensional perturbations in cylindrically symmetric mean flows:

$$\frac{dE}{dt} = -\int_0^\infty \left[\overline{u^2}\frac{\partial U}{\partial r} + \overline{v^2}\frac{U}{r} + \overline{uv}\left(\frac{\partial V}{\partial r} - \frac{V}{r}\right)\right] 2\pi r dr \tag{7.2}$$

where the overbars refer to the azimuthal averages. For convenience we have neglected the viscous damping terms. Another useful form of this equation can be found by integrating the first and third terms in the integrand of (7.2) by parts:

$$\frac{dE}{dt} = \int_0^\infty \left[\left(\frac{\partial}{\partial r}\overline{u^2} + \frac{\overline{u^2}}{r}\right)U - \overline{v^2}\frac{U}{r} + \overline{u'\zeta'}V\right] 2\pi r dr \tag{7.3}$$

where we have used (7.1) to simplify the third term in the integrand. This equation has a clear

physical interpretation since the first and third terms now represent the products of the eddy flux divergences (which are accelerations) multiplied by the mean flow velocities, thereby indicating the interaction of the perturbations with the mean flow. The second term represents the work done by the mean flow against the centripetal forces associated with the perturbation azimuthal velocities. Note that it is always positive when U is negative. The third term shows the direct interaction of the eddy flux divergence with the mean azimuthal flow. Since the rate of change of energy of the perturbations is equal and opposite to the rate of change of energy of the mean flow, this term clearly shows how upgradient (downgradient) momentum fluxes cause an increase (decrease) in the kinetic energy of the mean flow.

The eddy flux divergence of azimuthal momentum associated with the k=1 IO in the one-celled vortex is shown in Figure 19a. We can see that the immediate effect of the perturbation is to decelerate the mean flow inside r_{max} and to accelerate the flow outside r_{max}. The accumulated forcing of this perturbation over its lifetime can be found by simultaneously integrating the evolution of the perturbation (4.13) and the rate of change of the mean flow (7.1). We performed this integration from t=0 to t=1000, during which the energy of this perturbation decreased from E=1 to E=0.005. The accumulated forcing on the mean flow is shown in Figure 19b, where we can see that the net effect of the wave-mean flow interaction for this perturbation over its lifetime is to decrease the azimuthal velocity in the vicinity of r=1 and to increase it near r=0 and near r=2. [Note: this result should not be confused with the actual deviation of the mean flow velocities. The symmetric perturbations to the vortex flow caused by the eddy flux divergences will themselves evolve according to an advection-diffusion equation similar to (3.6). The behavior of these perturbations will be addressed in a future paper.]

The same calculation for the k=2 IO in the one-celled vortex gives a different result. While

we can see in Figure 20a that the instantaneous effect at t=0 of this structure is to decelerate the mean flow at r=1 (as it should be so that the mean flow energy is decreasing), the long term effect shown in Figure 20b is to accelerate the flow near r=1, such that the kinetic energy of the mean flow actually increases rather than decreases. Why is this result different? Shepherd (1985) and Farrell and Ioannou (1993a) have shown for inviscid linear shear flows that all perturbations, regardless of their initial configuration, are sheared over and give their energy to the mean flow via eddy fluxes. Equivalent results were found by Carr and Williams (1989) and Nolan (1996) for vortex flows with $1/r$ velocity profiles. Thus the net effect of any perturbation to these flows will ultimately be to increase the kinetic energy of the mean flow. However, if the mean flow has a background vorticity gradient, the transient perturbations may excite neutral or nearly neutral modes (also known as "coherent structures"), such as the k=1 LDM, which then serve as a trap for perturbation kinetic energy. In this case, the energy of transiently growing perturbations is never returned to the mean flow, but rather lost through dissipation of the perturbation instead. Our results here for the k=1 and k=2 IOs in the one-celled vortex are examples of each of these two possible outcomes.

In the two-celled vortex, the change in sign of the background vorticity gradient lends to the persistence or growth of coherent structures at all wavenumbers. Through investigation of many different initial conditions, it appears to us *any* perturbation initially configured to project favorably onto the LDM ultimately leads to a decrease in the kinetic energy of the mean flow. However, perturbations *can* be chosen that will ultimately lead to an increase in the kinetic energy in the mean flow. This is demonstrated in Figure 21, where we have used as an initial condition the complex conjugate of the k=11 IO in the two-celled vortex. Taking the complex conjugate causes the perturbation to spiral in the reverse direction, so that the initial eddy momentum flux is

maximally upgradient rather than maximally downgradient. Since the k=11 LDM is not as persistent as those at lower wavenumbers, the structure is sheared over and the final result is that there is a net upgradient flux of momentum and an increase in mean flow kinetic energy. For all lower wavenumbers with this special initial condition the opposite result was found.

7.2 The effects of radial inflow and the associated deformation

The two vortex flows we have defined have cylindrical deformation fields which have two distinct effects on the perturbation vorticities. Firstly, the radial inflow advects the perturbation vorticity into the vortex core (and outward from the axis in the two-celled vortex). Secondly, the associated deformation field can cause either vorticity amplification (through stretching) or vorticity decay (through compression).

A comparison of the amplification rate due to vortex stretching with the actual transient or unstable growth rates suggests that the stretching/amplification associated with the radial inflow does play a role in the dynamics. For example, the maximum energy growth rates in both the one-celled and two celled vortices were on the order of 0.5, while the vorticity amplification rates were on the order of 0.005 for the one-celled vortex (see Figure 1c) and on the order of 0.05 for the two-celled vortex (see Figure 2c). Since the energy growth is equal to twice the amplification rate, this suggests the amplification may cause as much as 20% of the energy growth of perturbations in the two-celled vortex. A more quantitative evaluation is shown in Figure 22ab, where we have recalculated the eigenvalues of the LDMs and the IOs of the two-celled vortex while leaving out the stretching term **S** in the time evolution operator (4.14). While the overall amplificaton rates are about 20% less than before, it is surprising to see that wavenumber k=2 appears to have been destabilized! Examination of this newly unstable k=2 LDM (not shown) revealed that it was simply a lower wavenumber version of the unstable structures seen for k=3 and k=5 (see Figure 6). It

is difficult to understand from an energy standpoint why removing the stretching term would destabilize the lower wavenumbers, since we can see from Figure 2c that in the transition zone, where the vorticity gradient changes sign and the instability mechanism occurs, the stretching term is positive and so must be amplifying the vorticity in this region.

An equally important issue is the extent to which the vorticity advection caused by the radial inflow makes the results we have seen so far different from the many previous analyses of vortex flows without radial inflow. With this in mind we have recalculated the real parts of the eigenvalues of the LDMs for both the one- and two-celled vortices with both the radial velocity field and the associated deformation set to zero. For the one celled vortex, we found nearly identical results, except that without the radial inflow the k=1 LDM was even more persistent, the real part of it's eigenvalue having changed from -2.5×10^{-4} to -2.65×10^{-6}. In the case of the two celled votex, we observe in Figure 23a that the vortex has been destabilized now for *both* azimuthal wavenumbers k=1 and k=2.

Although these results without the radial inflow are instructive, they are not particularly relevant to intense atmospheric vortices. There is sufficient dissipation in tornadoes and hurricanes such that when the vortex-sustaining convergent inflow ceases, the vortex rapidly dissipates. Therefore it is inappropriate to address the dynamics of these vortex profiles without the necessary radial inflow. A more pertinent issue to address is how the asymmetric dynamics of our model vortices change as the strength of the radial inflow increases or decreases, and as the azimuthal velocity field adjusts to be in balance with the convergent flow. In the case of the one-celled vortex, a weaker radial inflow results in a broader, weaker vortex, i.e, r_{max} increases and v_{max} decreases; a stronger radial inflow intensifies the vortex. In the case of the two-celled vortex, increasing the strength of the deformation field results in a sharper azimuthal velocity gradient in

the transition zone from the potential flow to the stagnant core.

As we have shown for the one-celled vortex, the important structures for wave-mean flow interaction are not the LDMs but rather the transiently growing optimals, particularly the global optimals. Therefore to determine the change in the potential for wave-mean flow interaction as the radial inflow varies, we have varied the strength of the radial inflow from half its original value to twice its original value, while recalculating the associated azimuthal velocity profile. For a radial inflow of half the original strength, we obtain an azimuthal velocity profile that is of the Burger's solution type but with an increased r_{max}=1.45 and a decreased v_{max}=0.5; for twice the radial inflow we have r_{max}=0.70 and v_{max}=1.01. For each of these new vortex solutions we have recalculated the maximum finite energy growth. Figure 24a shows that, for k=1 in the one-celled vortex, there is a huge increase in potential growth as the vortex is intensified, but then for still further increases in the radial inflow the maximum growth decreases. Figure 24b shows that for k=2 the maximum growth decreases drastically as the radial inflow is increased, with similar results for k=3. For still higher wavenumbers, the maximum growth decreased substantially both with increasing wavenumbers and with increasing radial inflow.

Why does increasing the radial inflow velocity suppress transient growth? Indeed, this might seem paradoxical since increasing the radial inflow increases the maximum deformation rate of the mean flow. However, the radial inflow also has the effect of advecting perturbation vorticity *through* the region of maximum shear, thereby limiting the extent of the wave-mean flow interaction. Thus we can see why in the one-celled vortex increasing the strength of the radial inflow can suppress transient growth for all wavenumbers.

We now proceed along the same line to investigate transient growth for stable wavenumbers in the two-celled vortex. Figure 25a shows the results of a similar investigation for k=1 and

Figure 25b shows the same for k=12. The latter results show a slow increase of the maximum transient growth with increasing radial velocities. The k=1 results show a rapid increase of the maximum transient growth, followed by a huge increase in the maximum growth after the radial velocities are multipled by a factor of 1.3. The maximum growth diverges at the multiplicative factor of 1.4 because the vortex becomes unstable at this point. Thus the rapid rise in maximum transient growth indicates the approach to the unstable regime and the importance of the persistence mechanism of nearly-neutral modes in amplifying transient growth in the nearly-neutral regime. Furthermore, this rapid rise in maximum total growth demonstrates that, as the vortex flow intensifies, the introduction of small perturbations will result in wave-mean flow equilibration and the appearance of coherent structures well before the instability criterion is met. The difference between these results and those of the one-celled vortex is due to the fact that the radial velocities carry vorticity perturbations *into*, rather than *through*, the region of maximum shear.

8 Summary and Conclusions

In this report we have studied the dynamics of asymmetric perturbations in two-dimensional vortex flows that are maintained by radial inflow. The results we have found regarding stability are consistent with previous work on vortices of various velocity profiles: the one-celled vortex is stable for all azimuthal wavenumbers, while the two-celled vortex has a finite range of unstable wavenumbers due to the change in sign of the vorticity gradient of the mean flow. We also demonstrated how the initial condition that leads to the greatest growth of the unstable modes are not the unstable modes themselves but rather the most unstable modes of the adjoint operator.

For all wavenumbers in both vortices the fastest instantaneous growth rates were shown to belong not to the LDMs but rather to the IOs. We also found that for stable wavenumbers substantial transient growth over finite times can occur for low-wavenumber perturbations in both the

one-celled and two-celled vortex. The energy source for transiently growing perturbations is the exchange of energy with the mean flow via eddy momentum fluxes.

While the immediate effect of all growing perturbations is to decrease the kinetic energy of the mean flow, we found that the net effect of these perturbations on the mean flow over their lifetimes varies from case to case. While most initially growing perturbations result in a long-term decrease in the mean flow kinetic energy for all wavenumbers in the two-celled vortex, and for wavenumber k=1 in the one-celled vortex, we found that most perturbations for k>1 in the one-celled vortex ultimately increased the kinetic energy of the mean flow.

The effect of the radial inflow, generally neglected in previous stability analyses, was also investigated. The vortex stretching caused by the associated deformation field was found to stabilize waveumber 2 perturbations in the two-celled vortex despite the fact that the effect of the deformation field is to amplify perturbation vorticity. It was also found that the combination of both advection and deformation associated with the radial inflow was necessary to stabilize the two-celled vortex to wavenumber 1 perturbations. More relevant to the case of vortices being maintained by a radial inflow with intensity varying in time, we examined how the wave-mean flow dynamics changed as the azimuthal velocity field was adjusted to be in balance with changing radial inflow velocities. In the case of one-celled vortices, we found that increasing the radial inflow could suppress transient growth of perturbations for all wavenumbers. For two-celled vortices, we found that increasing the radial velocities increases the maximum transient growth and ultimately destabilizes wavenumbers k=1 and k=2.

Throughout this investigation we have found that large transient growths in perturbation kinetic energy is limited to the lowest wavenumbers, particularly only k=1 for the one-celled vortex and both k=1 and k=2 for the two-celled vortex. Physically, k=1 perturbations correspond to a

linear displacement of some or all of the vorticity of the total flow. However, this translation is important since it corresponds to deviations in the path of the vortex, which has particularly important applications in the forecasting of hurricane tracks. It is generally observed that tornadoes do not travel in straight lines [see for example, Fuijita and Smith (1993)] and even laboratory vortices [Wan and Chang (1972); Lund and Snow (1993)] "wander" considerably, so it is possible that the transient growth and decay of wavenumber 1 perturbations is repsonsible for this phenomenon for both tornadoes and hurricanes. With this in mind we can see how generalized stability analysis could identify the characteristic features of disturbances which are most likely to causes significant changes in the path and intensity of tropical cyclones and tornadoes.

This report is the first in a series of steps which we hope will ultimately lead to a much deeper understanding of wave-mean flow dynamics in intense atmospheric vortices. This understanding will lead to a greater appreciation of the role that asymmetric processes play in the development, maintenance, and decline of these phenomena. In a future paper we will investigate the dynamics of these vortex systems when they are excited by a stochastic forcing term which is intended to model both the affects of the environmental forcings and the scattering of energy by non-linear terms. We will also allow the mean flow to change in time as predicted by the eddy flux divergences of the perturbations to investigate the equilibration process in both the stable and unstable regimes.

Acknowledgements

The authors would like to thank P. Ioannou, M. Montgomery, and T. DelSole for many helpful discussions. We would also especially like to thank D. Adalsteinsson for helping us to make tremendous improvements in the production and appearance of our contour plots. Preliminary work for this report was prepared as part of the Ph.D. thesis of D. Nolan while a student at Harvard University, during which he was supported by NSF Grant ATM-9216813 and NSF Grant 9623539; since Novemeber of 1996 D. Nolan has been supported by the U.S. Department of Energy under contract DE-AC03-76SF-00098 B. Farrell was supported by NSF Grant ATM-9216813 and NSF Grant 9623539.

References

Burgers, J. M., 1948: A mathematical model illustrating the theory of turbulence. *Adv. Appl. Mech.*, **1**, pp. 197-199.

Burggraf, O. R., K. Stewartson, and R. Belcher, 1971: Boundary layer produced by a potential vortex. *Phys. Fluids.*, **14**, pp. 1821-1833.

Butler, Kathy M., 1991: *Equilibration and Optimal Excitation in Viscous Shear Flow.* Ph.D. Thesis, Division of Applied Sciences, Harvard University, 133 pp.

----------, and Brian F. Farrell, 1992: Three dimensional optimal perturbations in viscous shear flows. *Phys. Fluids A*, **5**, pp. 1390-1393.

Carr, L. E. III, and R. T. Williams, 1989: Barotropic vortex stability to perturbations from axisymmetry. *J. Atmos. Sci.*, **46**, pp. 3177-3191.

Case, K. M., 1960: Stability of plane Couette flow. *Phys. Fluids*, **8**, pp. 143-148.

Chang, Tien Sun, and Walter K. Sartory, 1967: Hydromagnetic stability of dissipative flow between rotating permeable cylinders. *J. Fluid Mech.*, **27**, pp. 65-79.

Farrell, Brian, 1988: Optimal excitation of neutral rossby waves. *J. Atmos Sci.*, **45**, pp. 163-172.

----------, 1989: Transient development in confluent and difluent flow. *J. Atmos. Sci.*, **46**, pp. 3279-3288.

Farrell, Brian F., and Petros J. Ioannou, 1993a: Stochastic forcing of perturbation variance in unbouded shear and deformation flows. *J. Atmos. Sci.*, **50**, pp. 200-211.

----------, and ----------, 1993b: Optimal excitation of three-dimensional perturbations in viscous constant shear flow. *Phys. Fluids A*, **5**, pp. 1390-1400.

----------, and ----------, 1996: Generalized stability theory. Part I: Autonomous operators. To appear in *J. Atmos. Sci.*

Flierl, Glenn R., 1988: On the instability of geostrophic vortices. *J. Fluid Mech.*, **197**, pp. 349-388.

Fujita, T. T., and Smith, B. E., 1993: Aerial survey and photography of tornado and micorburst damage. In *The Tornado: its Structure, Dynamics, Prediction, and Hazards*, C. Church, *et. al.*, eds., American Geophysical Union, Washington, D.C., 1993.

Gall, R. L., 1983: A linear analysis of the multiple vortex phenomenon in simulated tornadoes. *J. Atmos. Sci.*, **40**, pp. 2010-2024.

----------, 1985: Linear dynamics of the multiple-vortex phenomenon in tornadoes. *J. Atmos. Sci.*, **42**, pp. 761-772.

Guinn, Thomas A., and Wayne H. Schubert, 1993: Hurricane sprial bands. *J. Atmos. Sci.*, **50**, pp. 3380-3403.

Howard, Louis N., 1972: Bounds on flow quantities. *Ann. Rev. Fluid Mech.*, **4**, pp. 473-493.

Howells, Peter C., Richard Rotunno, and Roger K. Smith, 1988: A comparitive study of atmosheric and laboratory analogue numerical tornado-vortex models. *Q. J. Roy. Met. Soc.*, **114**, pp. 801-822.

----------, and A. S. Gupta, 1962: On the hydrodynamic and hydromagnetic stability of swirling flows. *J. Fluid Mech.*, **14**, pp. 463-476.

Joseph, D. D., 1976: *Stability of Fluid Motions I.* Springer-Verlag, Berlin.

Kallenbach, R. J., and Montgomery, M. T., 1995: Symmetrization and hurricane motion in an asymmetric balance model. *21st Conference on Hurricanes and Tropical Meteorology.* Americal Meteorological Society, pp. 103-105.

Leibovich, S., and K. Stewartson, 1983: A sufficient condition for the instability of columnar vortices. *J. Fluid Mech.*, **126**, pp. 335-356.

Lewellen, W. S., and D. C. Lewellen, 1997: Large-eddy simulation of a tornado's interaction withthe surface. *J. Atmos. Sci.*, **54**, pp. 581-605.

Michalke, Alfons, and Adalbert Timme, 1967: On the inviscid instability of certain two-dimensional vortex-type flows. *J. Fluid. Mech.*, **29**, pp. 647-666.

Molinari, J., 1992: Environmental controls on eye wall cycles and intensity change in Hurricane Allen (1980). *ICSU International Symposium on Tropical Cyclone Disasters*, October 12-16, Beijing.

Montgomery, Michael T., and Randall J. Kallenbach, 1996: A theory for vortex Rossby waves and its application to spiral bands and intensity changes in hurricanes. Submitted to *Q. J. Roy. Met. Soc.*

Nolan, David S., 1996: *Axisymmetric and Asymmetric Vortex Dynamics in Convergent Flows.* Ph.D. Thesis, Department for Earth and Planetary Sciences, Harvard University.

Orr, W. Mc'F., 1907: Stability or instability of the steady motions of a perfect liquid. *Proc. Roy. Irish Acad.*, **27**, pp. 9-69.

Peng, Melinda S., and R. T. Williams, 1991: Stability analysis of barotropic vortices. *Geophys. and Astrophys. Fluid Dynamics*, **58**, pp. 263-283.

Rayleigh, Lord, 1880: On the stability and instability of certain fluid motions. *Proc. London Math. Soc.*, **11**, pp. 57-70.

Robinson, A. C., and P. G. Saffman, 1984: Stability and structure of stretched vortices. *Stud. Appl. Math.*, **70**, pp. 163-180.

Rott, N., 1958: On the viscous core of a line vortex. *Z. Agnew Math. Mech.*, **9**, pp. 543-553.

Rotunno, Richard, 1978: A note on the stability of a cylindrical vortex sheet. *J. Fluid Mech.*, **87**, pp. 761-771.

Shapiro, Lloyd J., 1992: Hurricane vortex motion in a three-layer model. *J. Atmos. Sci.*, **108**, pp. 401-421.

Shepherd, Theodore G., 1985: Time development of small disturbances to plane Couette flow. *J. Atmos. Sci.*, **42**, pp. 1868-1871.

Smith, Gerald B. II, and Michael T. Montgomery, 1995: Vortex axisymmetrization: Dependence on azimuthal wavenumber or asymmetric radial structure changes. *Q. J. Roy. Met. Soc.*, **121**, pp. 1615-1650.

Smith, R. K., and H. C. Weber, 1993: An extended analytic theory of tropical-cyclone motion in a a barotropic shear flow. *Q. J. R. Meteorol. Soc.*, **119**, pp. 1149-1166.

Staley, D. O., 1985: Effect of viscosity on inertial instability in a tornado vortex. *J. Atmos. Sci.*, **42**, pp. 293-297.

----------, and R. L. Gall, 1979: Barotropic instability in a tornado vortex. *J. Atmos. Sci.*, **36**, pp. 973-981.

----------, and ----------, 1984: Hydrodynamic instability of small eddies in a tornado vortex. *J. Atmos. Sci.*, **41**, pp. 422-429.

Steffens, Jerry L., 1988: The effect of vorticity-profile shape on the instability of a two-dimensional vortex. *J. Atmos. Sci.*, **45**, pp. 254-259.

Thompson, W., 1887: Stability of fluid motion: rectilinear motion of viscous fluid between two parallel planes. *Phil. Mag.*, **24**, 188-196.

Wan, C. C., and C. C. Chang, 1972: Measurement of the velocity field in a simulated tornado-like vortex using a three-dimensional velocity probe. *J. Atmos. Sci.*, **29**, pp. 116-127.

Willoughby, H. E., 1992: Linear motion of a shallow-water barotropic vortex as an initial-value problem. *J. Atmos. Sci.*, **49**, pp. 2015-2031.

----------, 1995: Normal-mode initialization of barotropic vortex motion models. *J. Atmos. Sci.*, **52**, pp. 4501-4514.

Figure Captions

Figure 1. Profiles of radial and azimuthal velocity for the idealized one-celled vortex: a) radial velocity; b) azimuthal velocity; c) negative horizontal divergence (stretching); d) vorticity gradient.

Figure 2. Profiles of radial and azimuthal velocity for the idealized two-celled vortex: a) radial velocity; b) azimuthal velocity; c) negative horizontal divergence (stretching); d) vorticity gradient.

Figure 3. Real parts of the eigenvalues of the LDM for azimuthal wavenumbers 1 through 12 in the one-celled vortex.

Figure 4. The LDMs for the first two azimuthal wavenumbers in the one-celled vortex: a) contours of vorticity for k=1; b) contours of streamfunction for k=1; c) contours of vorticity for k=2; d) contours of streamfunction for k=2. The contour intervals and decay rates (the real part of the eigenvalue) are indicated at the top of each plot.

Figure 5. Stability diagram for asymmetric perturbations on the two-celled vortex, showing the real parts of the LDMs for each azimuthal waveumber from k=1 to k=15.

Figure 6. Streamfunction and vorticity fields for the most unstable (least damped) perturbations at the first waveumber with instability, k=3, and the wavenumber with highest instability, k=5: a) k=3 vorticity; b) k=3 streamfunction; c) k=5 vorticity; d) k=5 streamfunction.

Figure 7. Angular velocity, or phase speed, of the LDMs for each azimuthal waveumber from k=1 to k=15.

Figure 8. The k=1 and k=2 IOs for the one-celled vortex: a) k=1 vorticity; b) k=1 streamfunction; c) k=2 vorticity; d) k=2 streamfunction. The contour intervals and energy growth rates (eigenvalues) are indicated at the top of each plot.

Figure 9. IO growth rates for k=1 to k=12 in the one-celled vortex.

Figure 10. Vorticity and streamfunction fields for the k=1 FTO for t=8.98, and its associated RFTO: a) k=1 FTO vorticity; b) k=1 FTO streamfunction; c) k=1 RFTO vorticity; d) k=1 RFTO streamfunction.

Figure 11. FTO growth versus allowed growth time in the one-celled vortex for a) azimuthal wavenumber k=1; b) k=2.

Figure 12. Initial and fully realized states of the global optimal for k=1 in the one-celled vortex: a) GO vorticity; b) GO streamfunction; c) RGO vorticity; d) RGO streamfunction.

Figure 13. Vorticity and streamfunction fields for the k=1 and k=2 IOs in the two-celled vortex: a) k=1 IO vorticity; b) k=1 IO streamfunction; c) k=2 IO vorticity; d) k=2 IO streamfunction.

Figure 14. Maximum instantaneous growth rates vs. wavenumber for the first 15 azimuthal wavenumbers in the two celled vortex.

Figure 15. FTO growth as a function of allowed growth time in the two-celled vortex: a) azimuthal wavenumber k=1; b) k=2.

Figure 16. Initial and maximal states of the GO for k=2 on the two-celled vortex: a) GO vorticity; b) GO streamfunction; c) RGO vorticity; d) RGO streamfunction.

Figure 17. Logarithms of the energies versus time of the LDM (solid), LDMA (dashed), and the t=5 FTO (dash-dot) for azimuthal wavenmber k=3 in the two-celled vortex.

Figure 18. Vorticity and streamfunction fields for the t=5 FTO and the LDMA for k=3 in the two-celled vortex: a) FTO vorticity; b) FTO streamfunction; c) LDMA vorticity; d) LDMA streamfunction.

Figure 19. a) The instantaneous eddy momentum flux divergence of the k=1 IO in the one-celled vortex; b) The accumulated total momentum flux divergence from t=0 to t=1000 for the k=1 IO.

Figure 20. a) The instantaenous eddy momentum flux divergence of the k=2 IO in the one-celled vortex; b) The accumulated total momentum flux divergence from t=0 to t=1000 for the k=2 IO.

Figure 21. a) The instantaenous eddy momentum flux divergence of the complex conjugate of the k=11 IO in the two-celled vortex; b) The accumulated total momentum flux divergence from t=0 to t=1000.

Figure 22. a) Real parts of the eigenvalues of the LDMs in the two-celled vortex and b) maximum instantaneous growth rates in energy in the two-celled vortex, when the stretching term has been removed from the vorticity evolution equation.

Figure 23. a) Real parts of the eigenvalues of the LDMs in the two-celled vortex and b) maximum instantaneous growth rates in energy in the two-celled vortex, when all terms associated with the radial inflow have been removed from the vorticity evolution equation.

Figure 24. Maximum transient growth in the one-celled vortex as a function of the relative strengths of the radial inflow velocity which maintains the vortex: a) for azimuthal wavenumber k=1; b) for k=2 (solid) and k=3 (dashed).

Figure 25. Maximum transient growth in the two-celled vortex as a function of the relative strengths of the radial inflow velocity which maintains the vortex: a) for azimuthal wavenumber k=1; b) for k=12. Note the domains are different in the two cases.

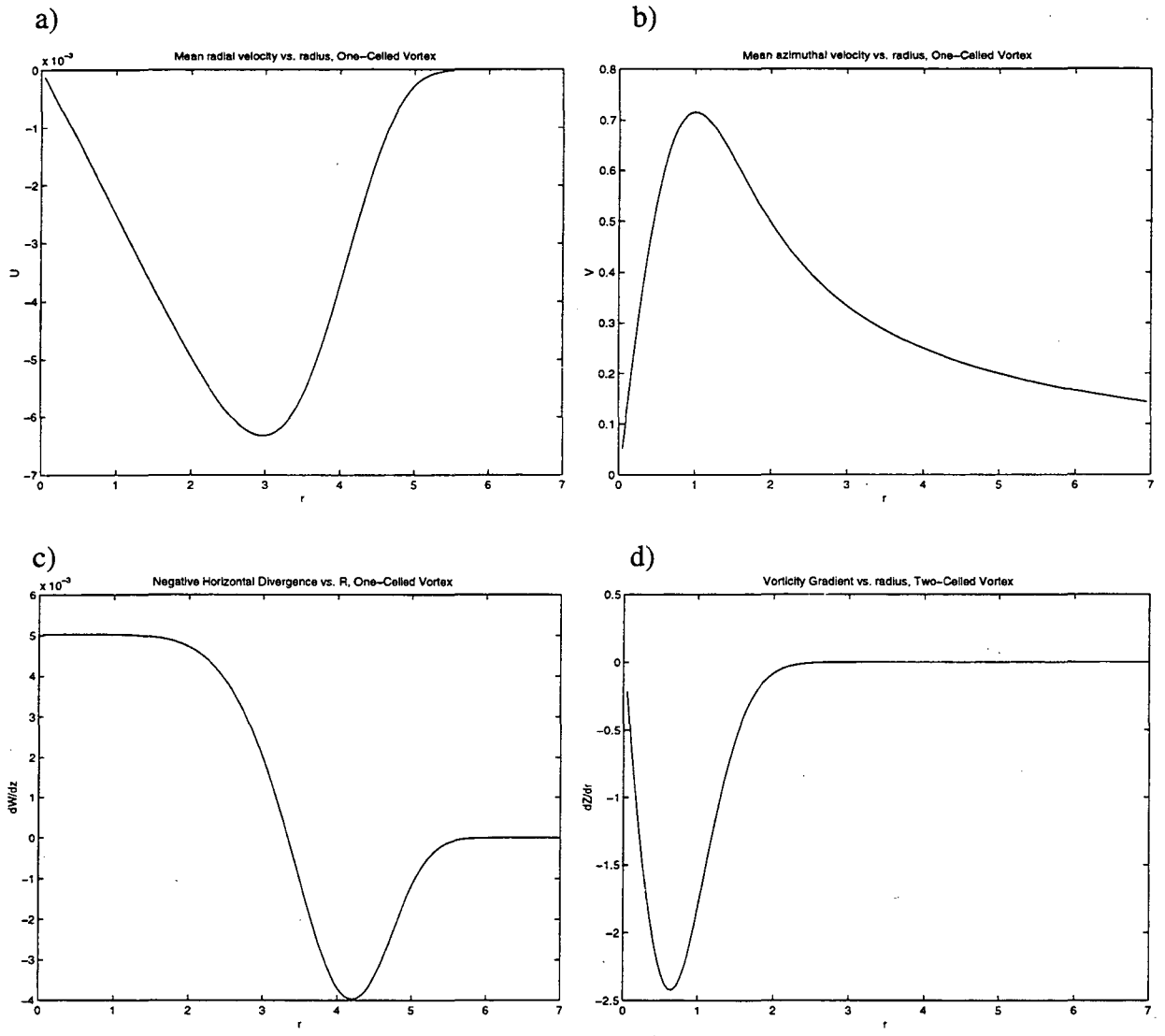

Figure 1 Profiles of radial and azimuthal velocity for the idealized one-celled vortex: a) radial velocity; b) azimuthal velocity; c) negative horizontal divergence (stretching); d) vorticity gradient.

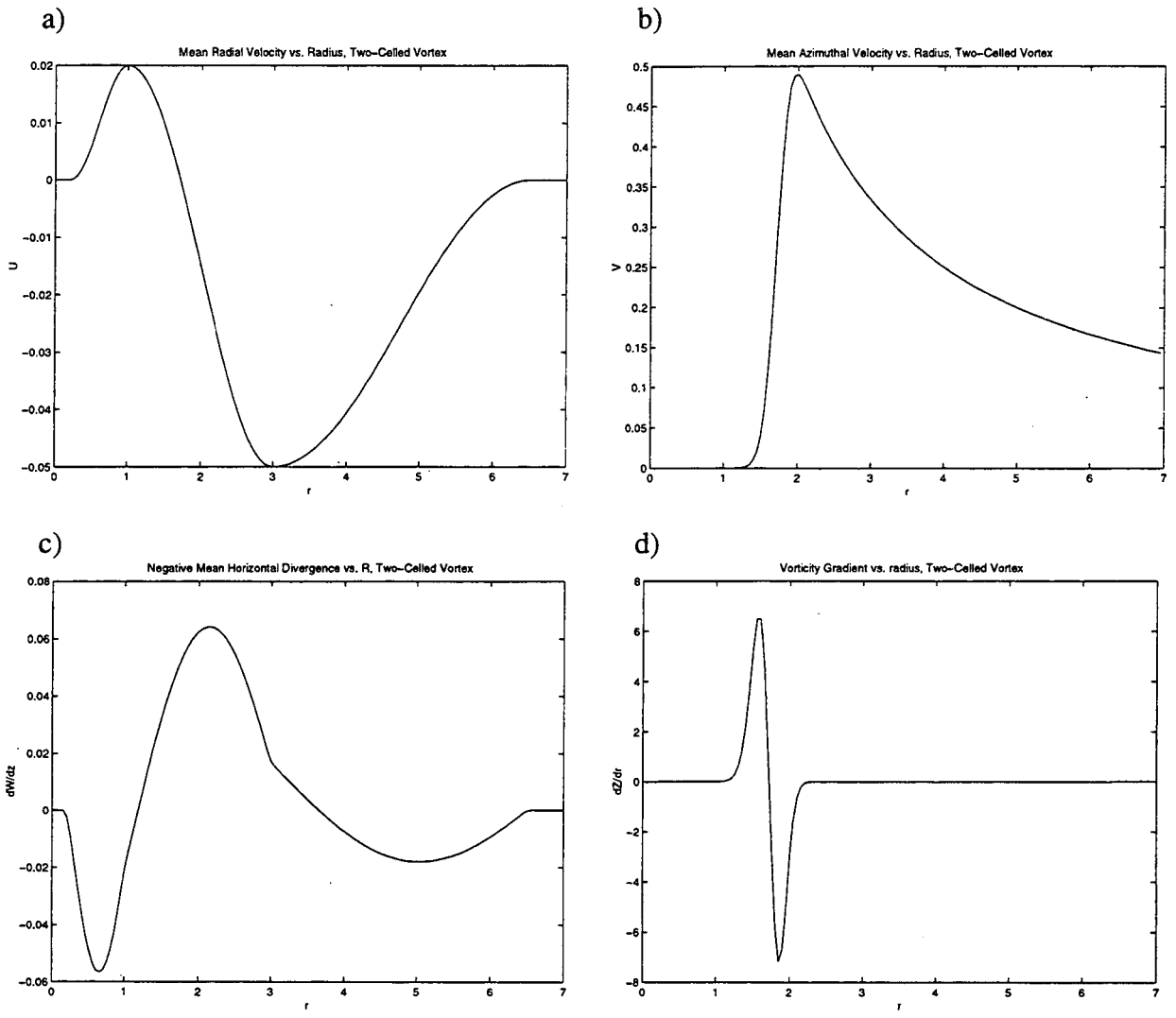

Figure 2 Profiles of radial and azimuthal velocity for the idealized two-celled vortex: a) radial velocity; b) azimuthal velocity; c) negative horizontal divergence (stretching); d) vorticity gradient.

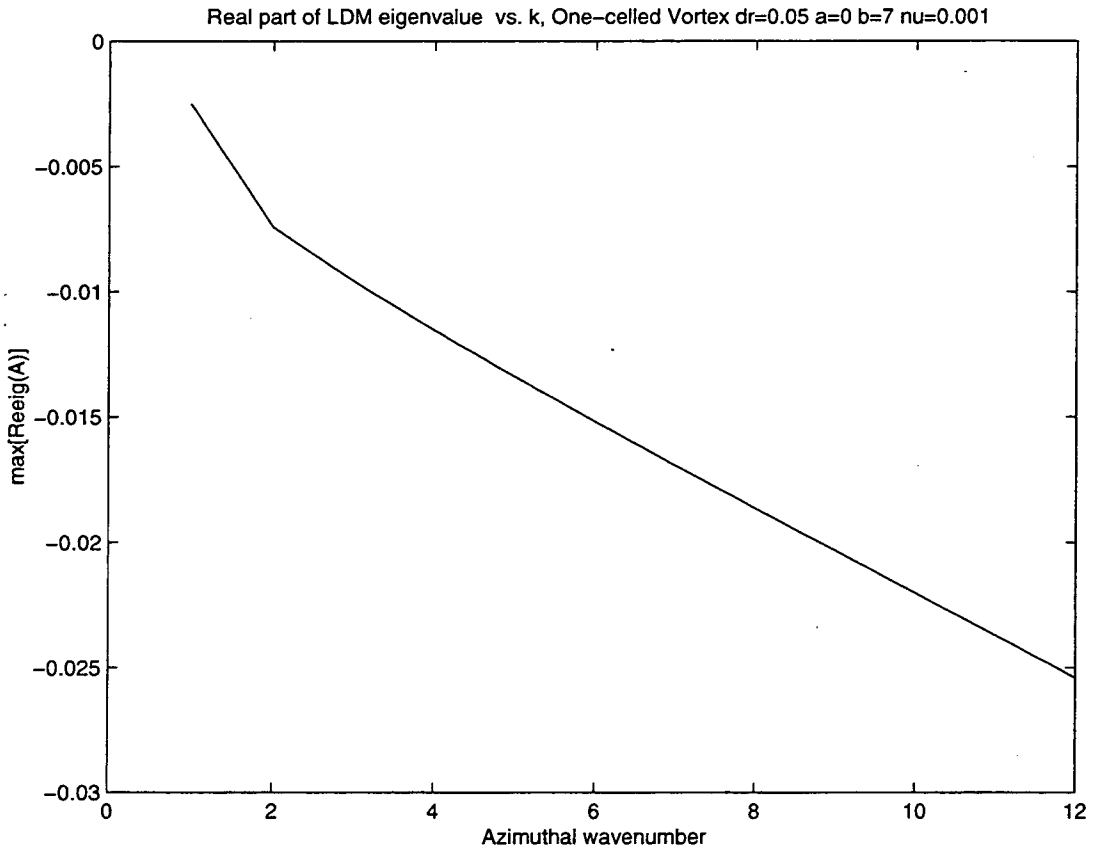

Figure 3 Real parts of the eigenvalues of the LDM for azimuthal wavenumbers 1 through 12 in the one-celled vortex.

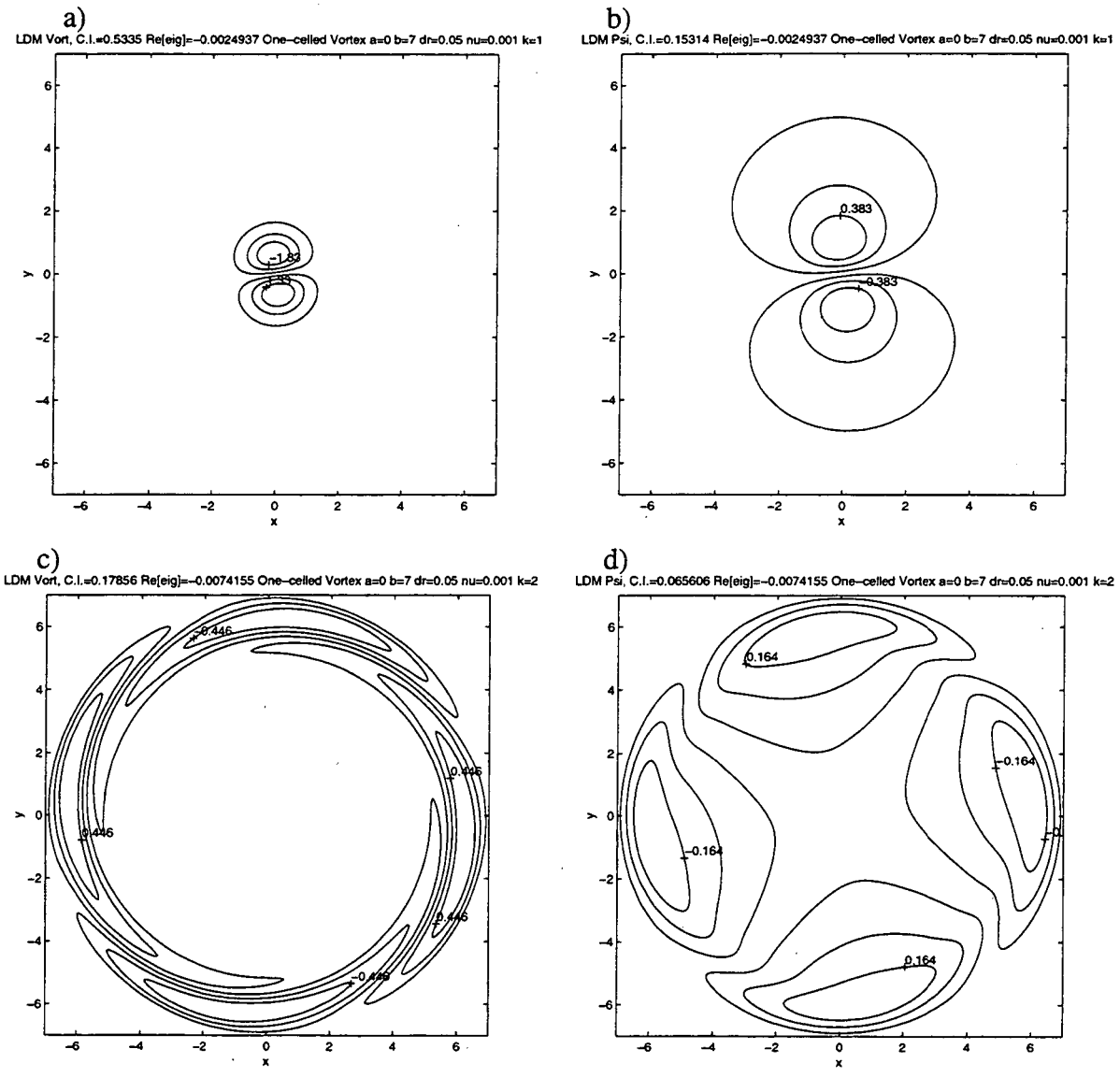

Figure 4 The LDMs for the first two azimuthal wavenumbers in the one-celled vortex: a) contours of vorticity for k=1; b) contours of streamfunction for k=1; c) contours of vorticity for k=2; d) contours of streamfunction for k=2. The contour intervals and decay rates (the real part of the eigenvalue) are indicated at the top of each plot.

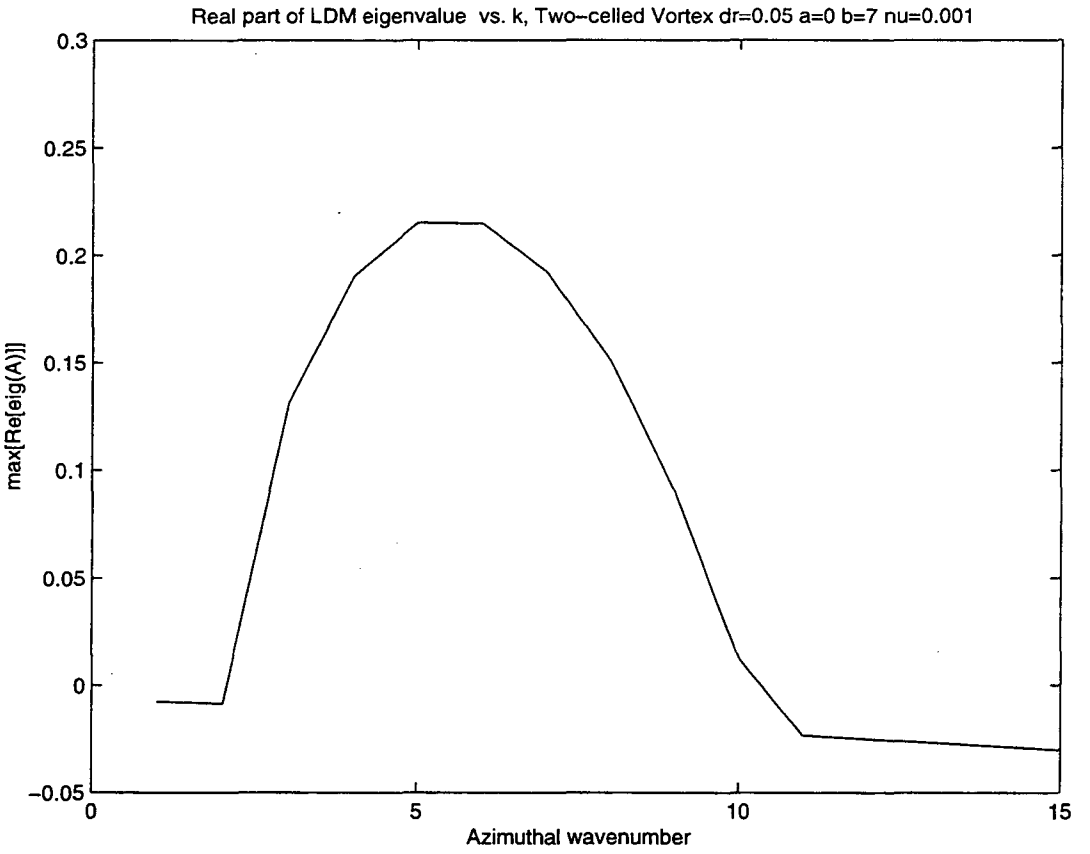

Figure 5 Stability diagram for asymmetric perturbations on the two-celled vortex, showing the real parts of the LDMs for each azimuthal waveumber from k=1 to k=15.

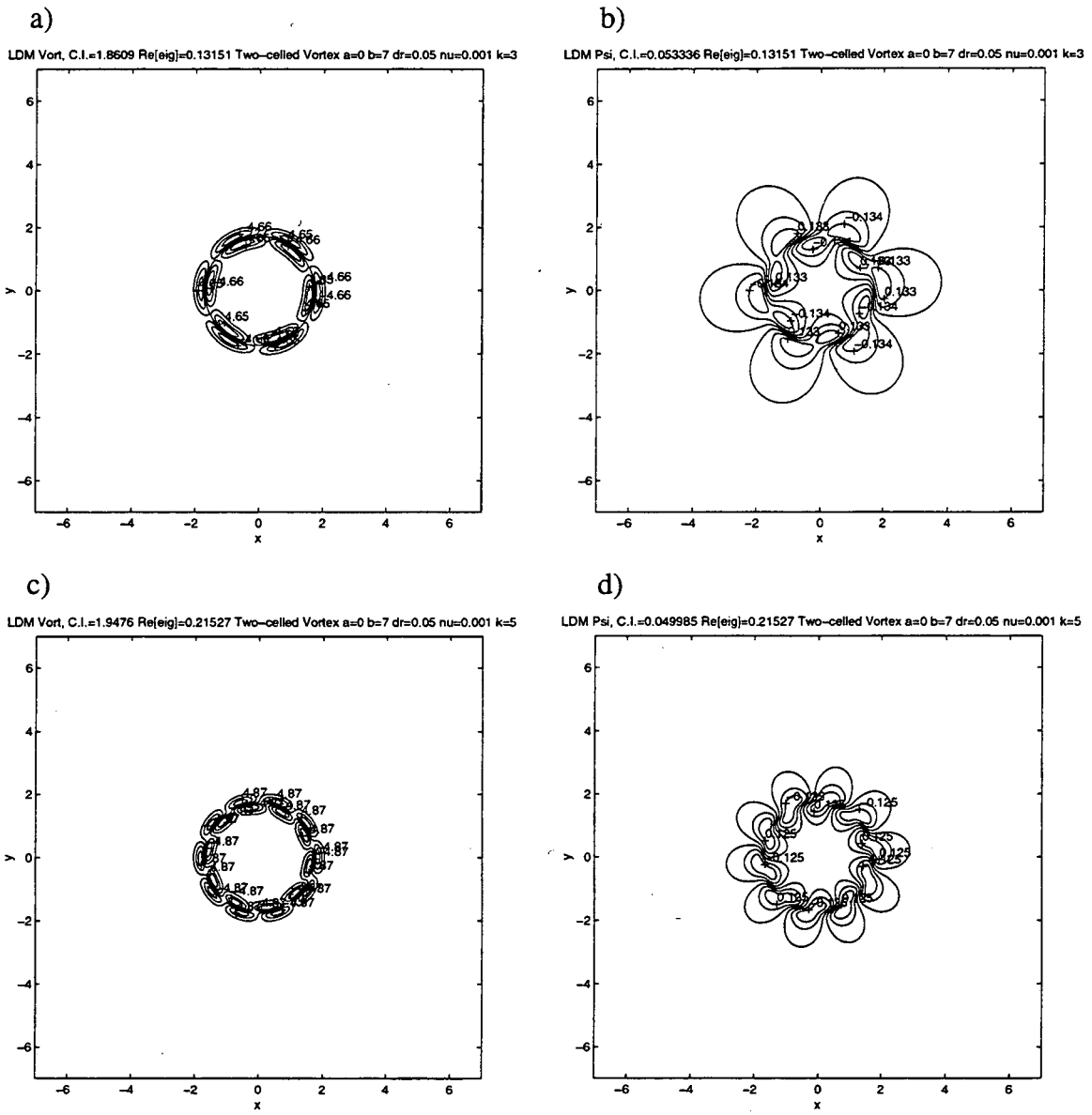

Figure 6 Streamfunction and vorticity fields for the most unstable (least damped) perturbations at the first waveumber with instability, k=3, and the wavenumber with highest instability, k=5: a) k=3 vorticity; b) k=3 streamfunction; c) k=5 vorticity; d) k=5 streamfunction.

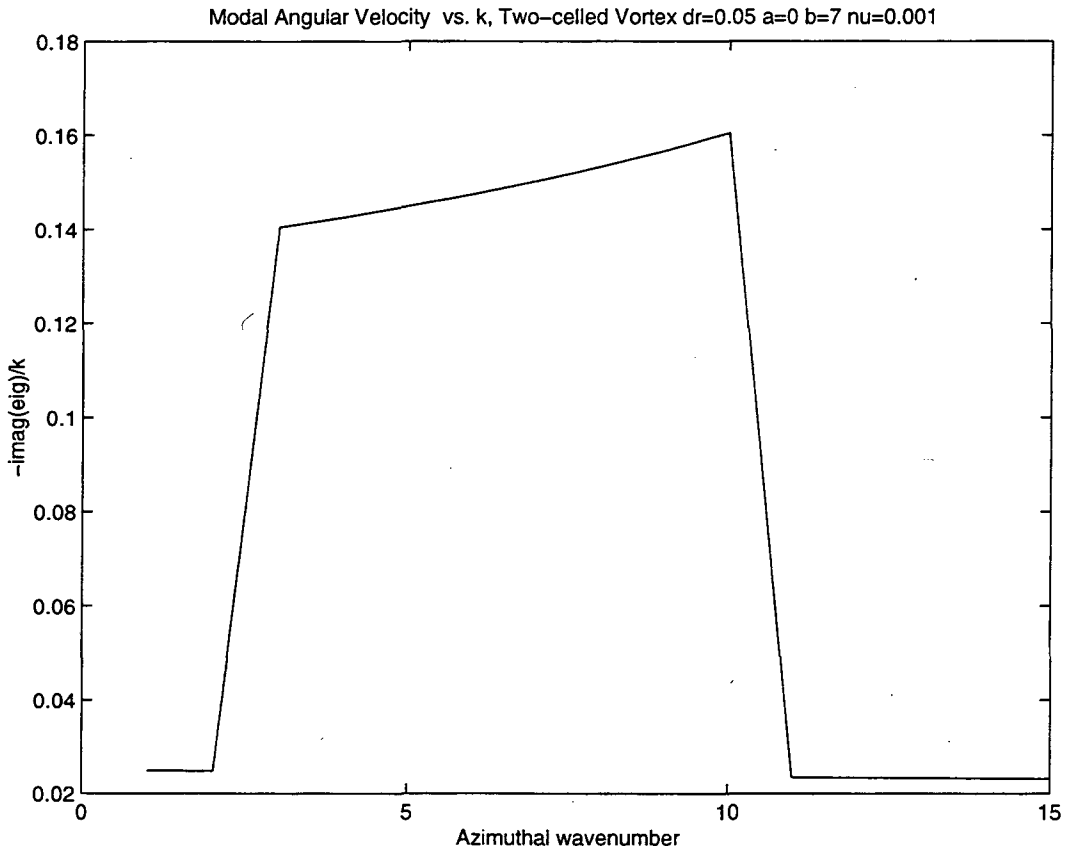

Figure 7 Angular velocity, or phase speed, of the LDMs for each azimuthal waveumber from k=1 to k=15.

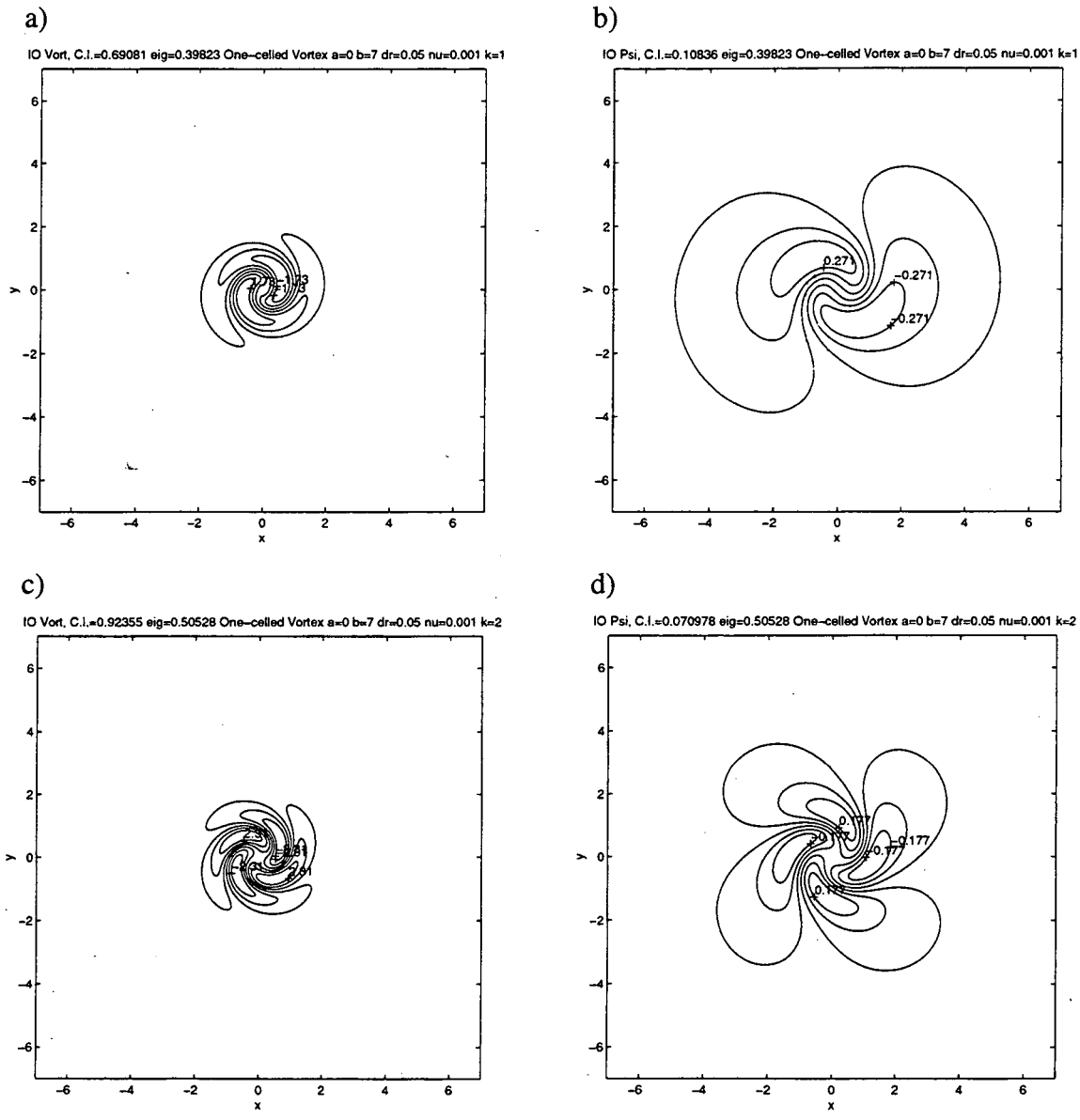

Figure 8 The k=1 and k=2 IOs for the one-celled vortex: a) k=1 vorticity; b) k=1 streamfunction; c) k=2 vorticity; d) k=2 streamfunction. The contour intervals and energy growth rates (eigenvalues) are indicated at the top of each plot.

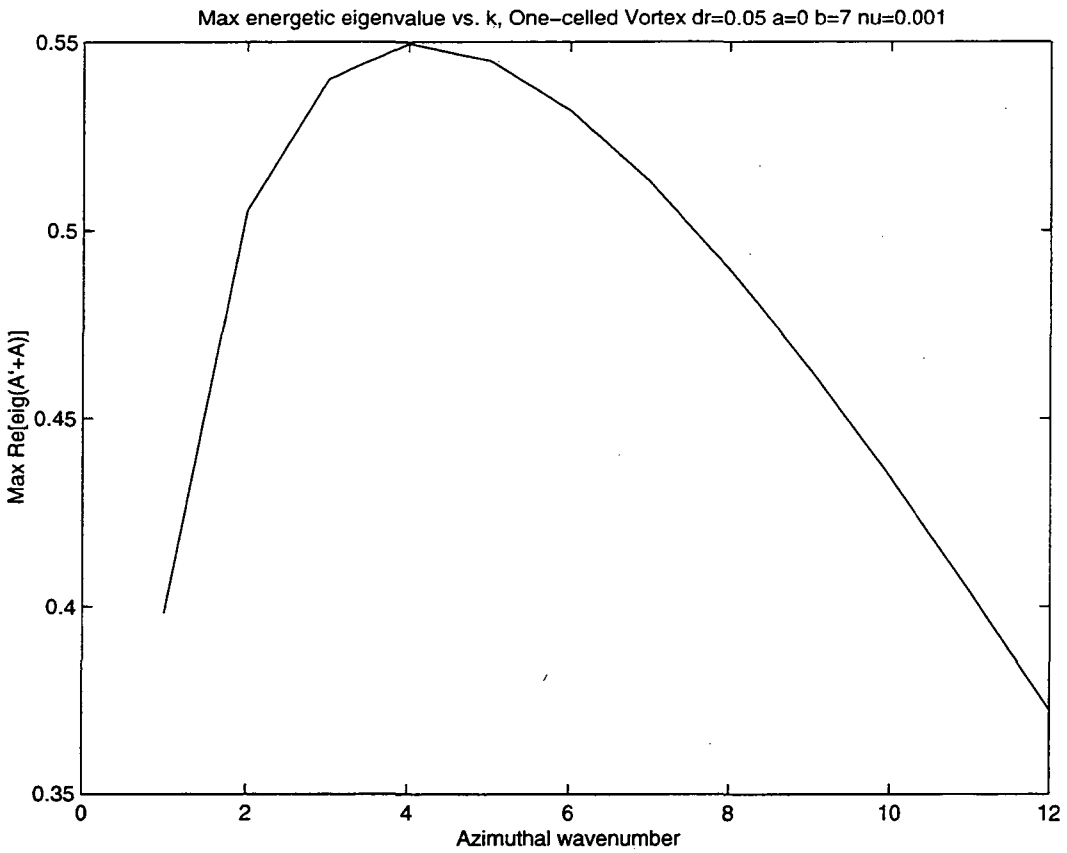

Figure 9 IO growth rates for k=1 to k=12 in the one-celled vortex.

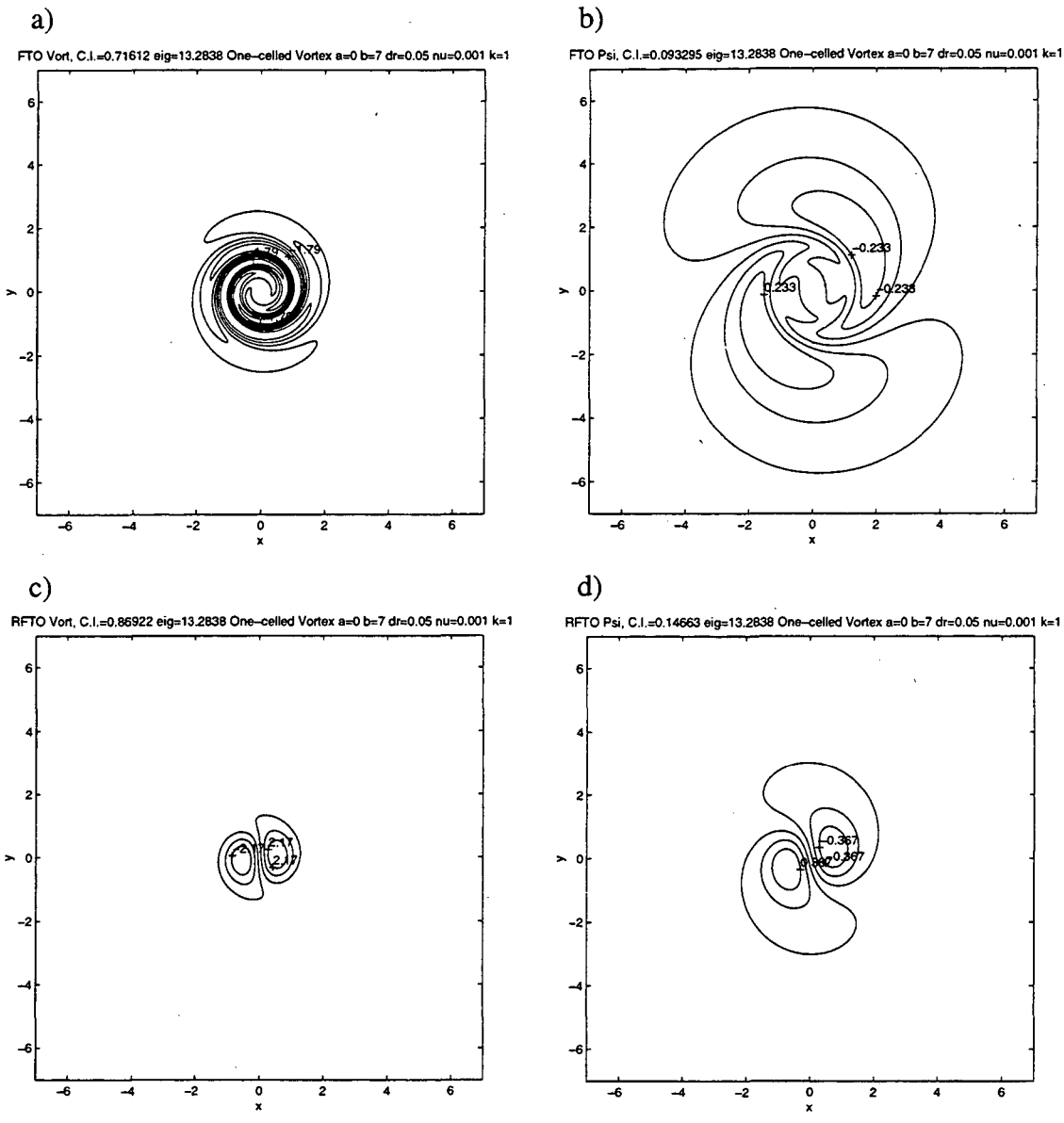

Figure 10 Vorticity and streamfunction fields for the k=1 FTO for t=8.98, and its associated RFTO: a) k=1 FTO vorticity; b) k=1 FTO streamfunction; c) k=1 RFTO vorticity; d) k=1 RFTO streamfunction.

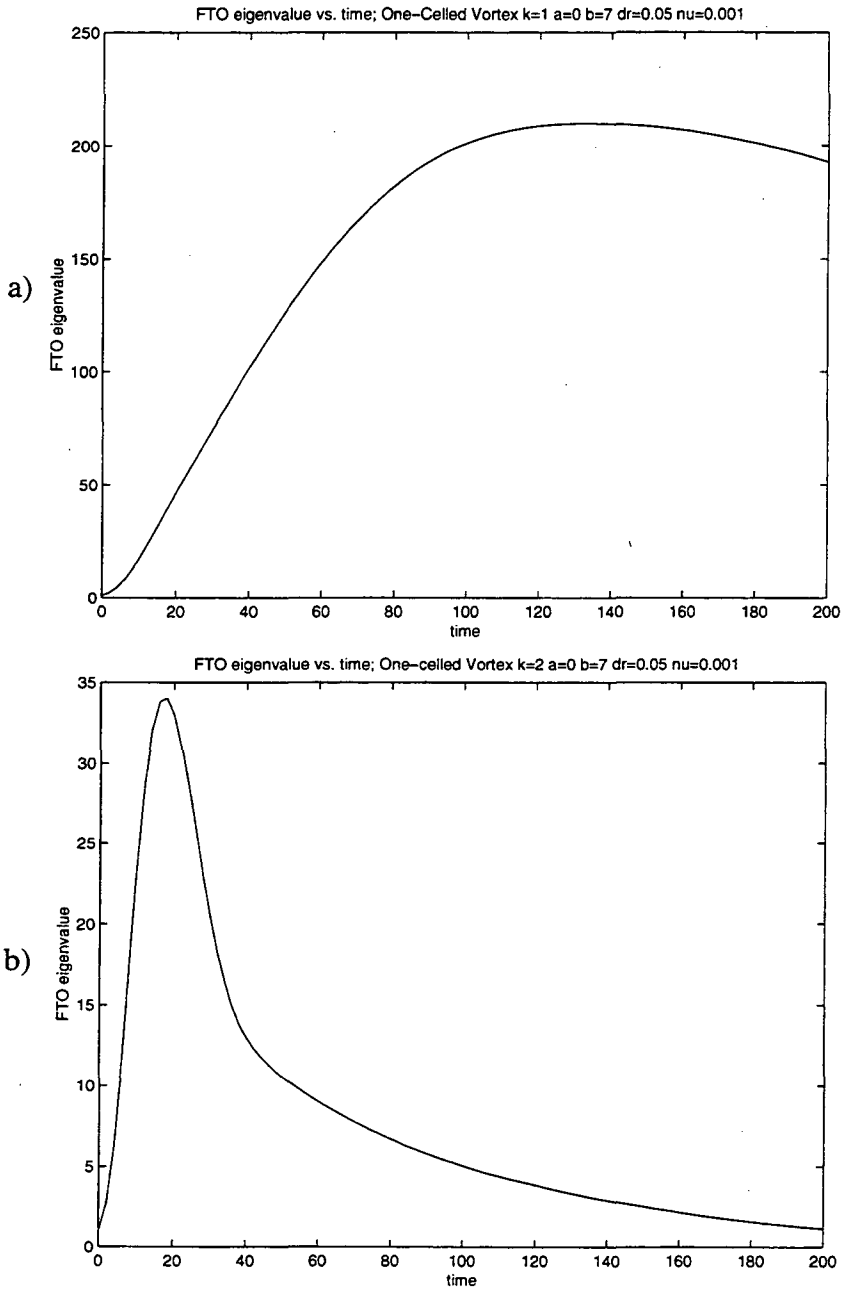

Figure 11 FTO growth versus allowed growth time in the one-celled vortex for a) azimuthal wavenumber k=1; b) k=2.

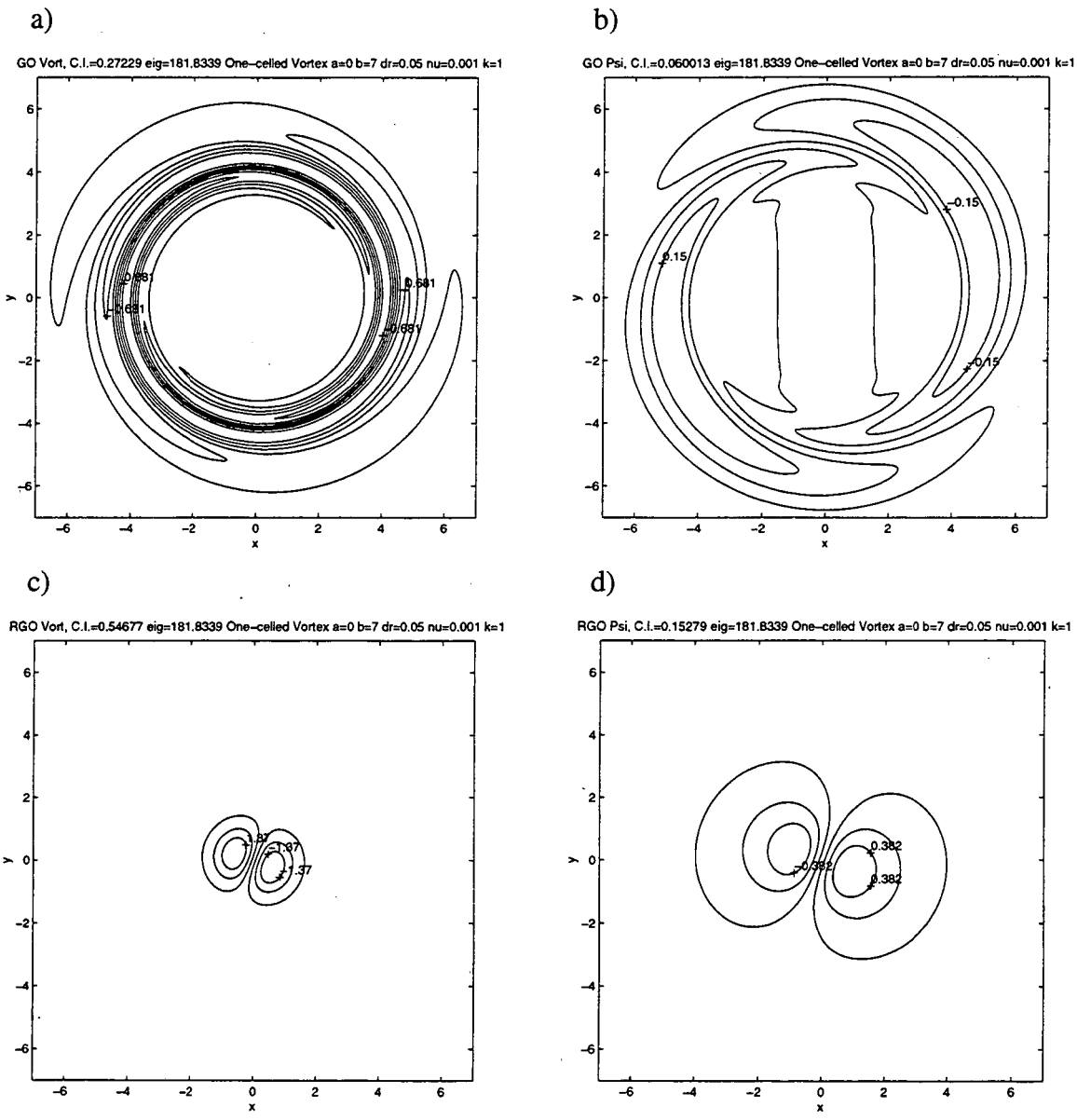

Figure 12 Initial and fully realized states of the global optimal for k=1 in the one-celled vortex: a) GO vorticity; b) GO streamfunction; c) RGO vorticity; d) RGO streamfunction.

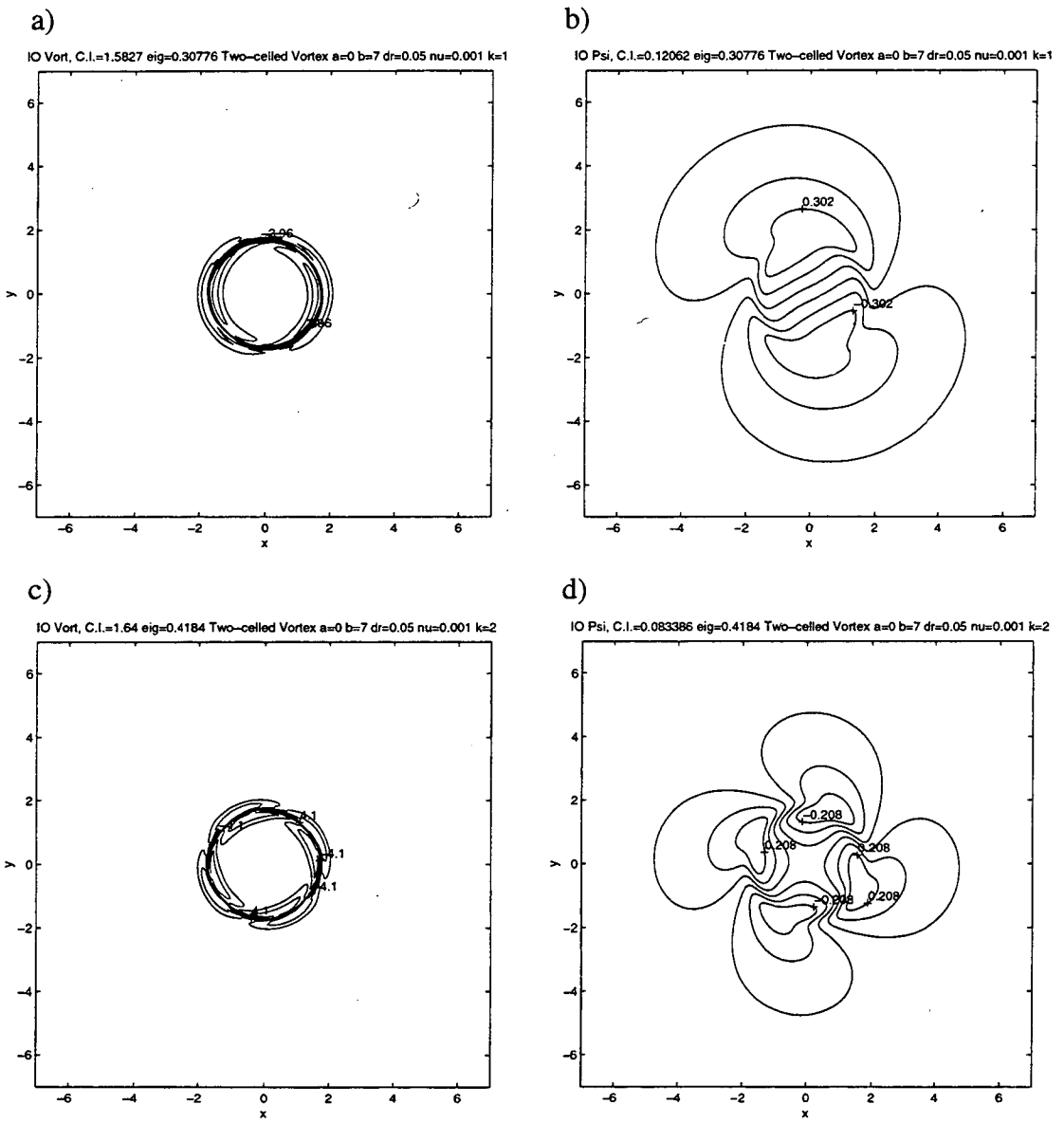

Figure 13 Vorticity and streamfunction fields for the k=1 and k=2 IOs in the two-celled vortex: a) k=1 IO vorticity; b) k=1 IO streamfunction; c) k=2 IO vorticity; d) k=2 IO streamfunction.

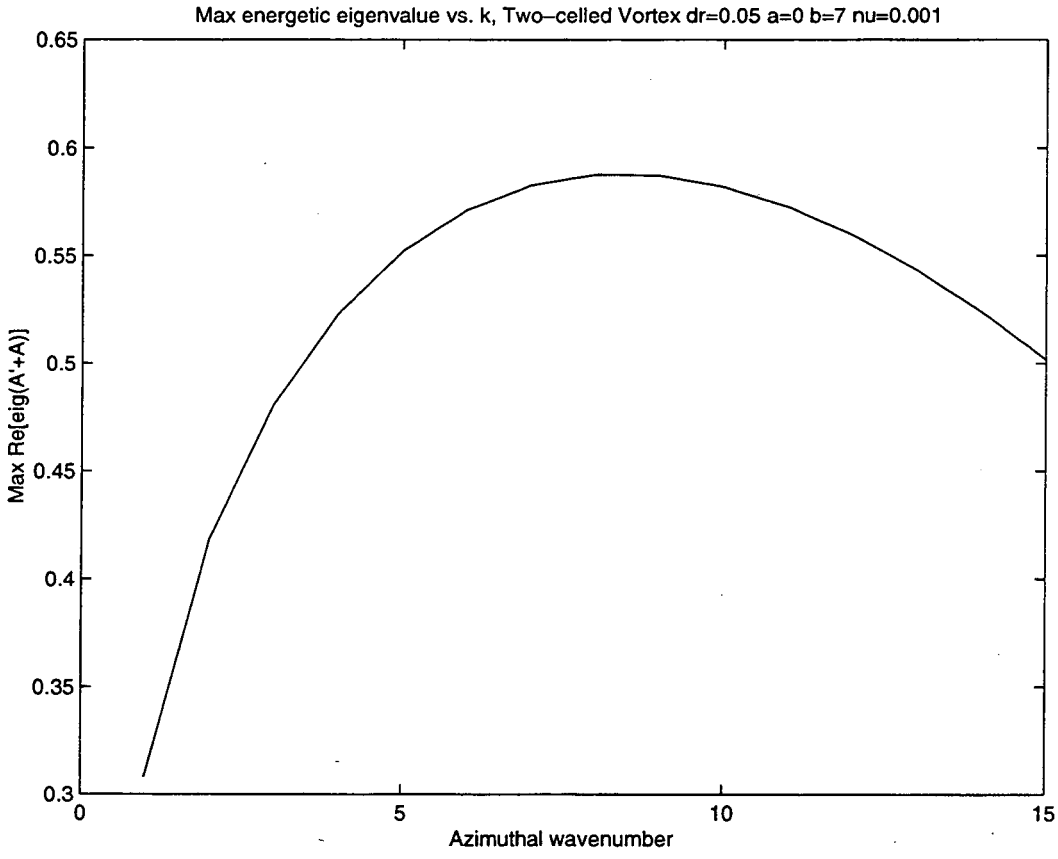

Figure 14 Maximum instantaneous growth rates vs. wavenumber for the first 15 azimuthal wavenumbers in the two celled vortex.

a)

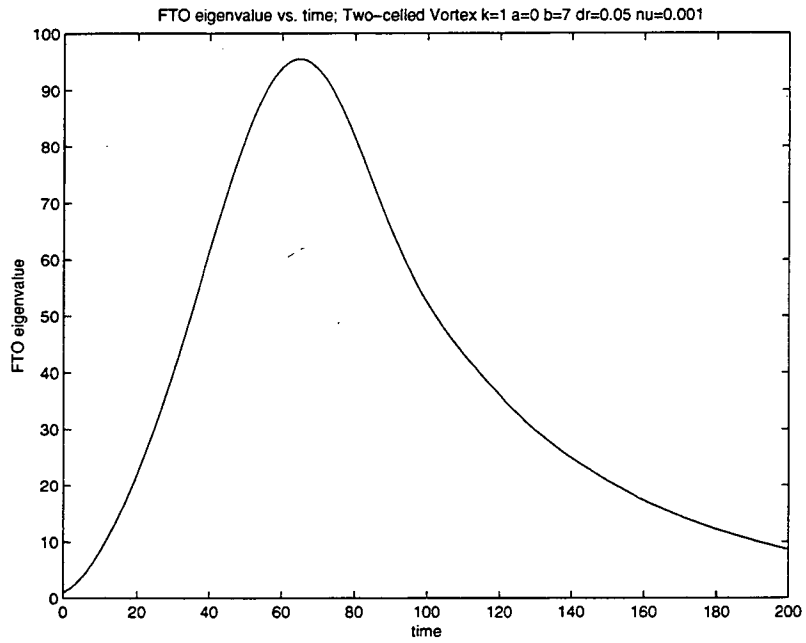

b)

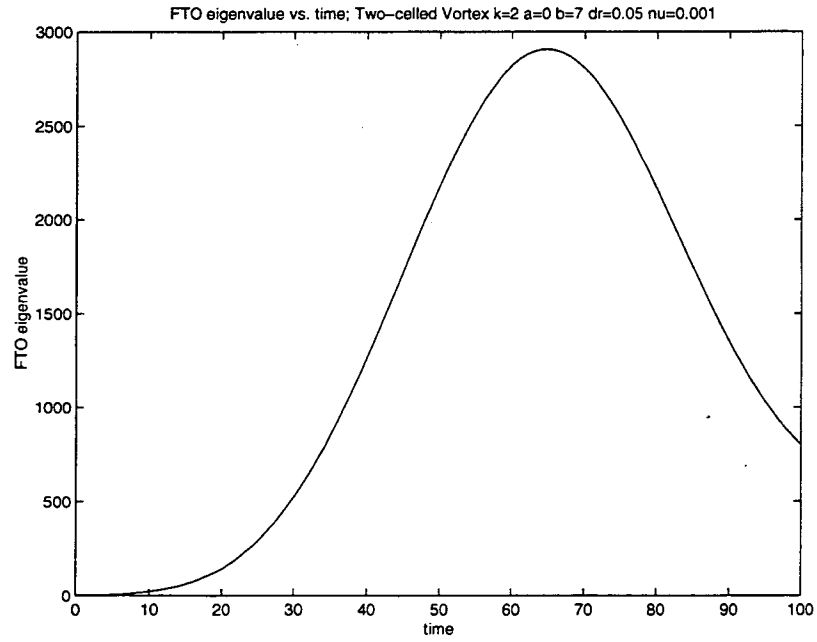

Figure 15 FTO growth as a function of allowed growth time in the two-celled vortex: a) azimuthal wavenumber k=1; b) k=2.

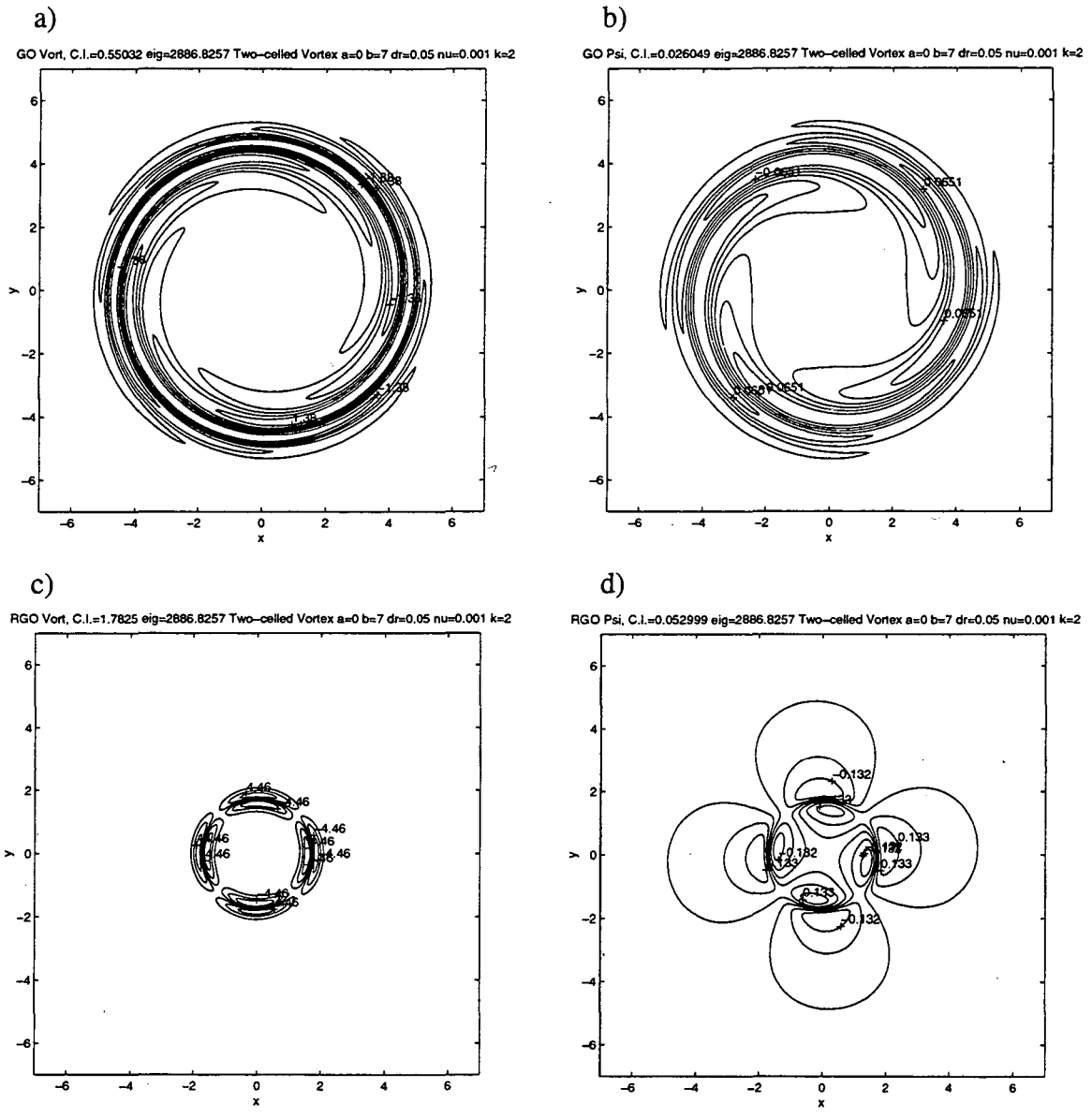

Figure 16 Initial and maximal states of the GO for k=2 on the two-celled vortex: a) GO vorticity; b) GO streamfunction; c) RGO vorticity; d) RGO streamfunction.

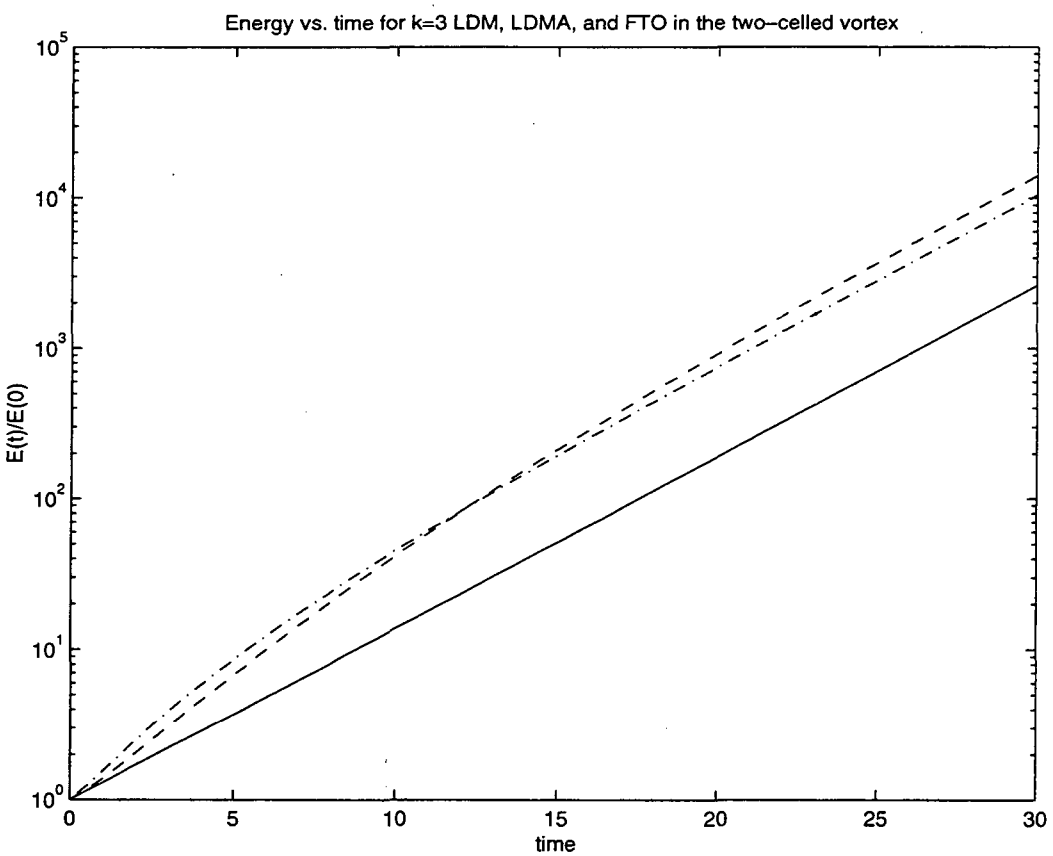

Figure 17 Logarithms of the energies versus time of the LDM (solid), LDMA (dashed), and the t=5 FTO (dash-dot) for azimuthal wavenmber k=3 in the two-celled vortex.

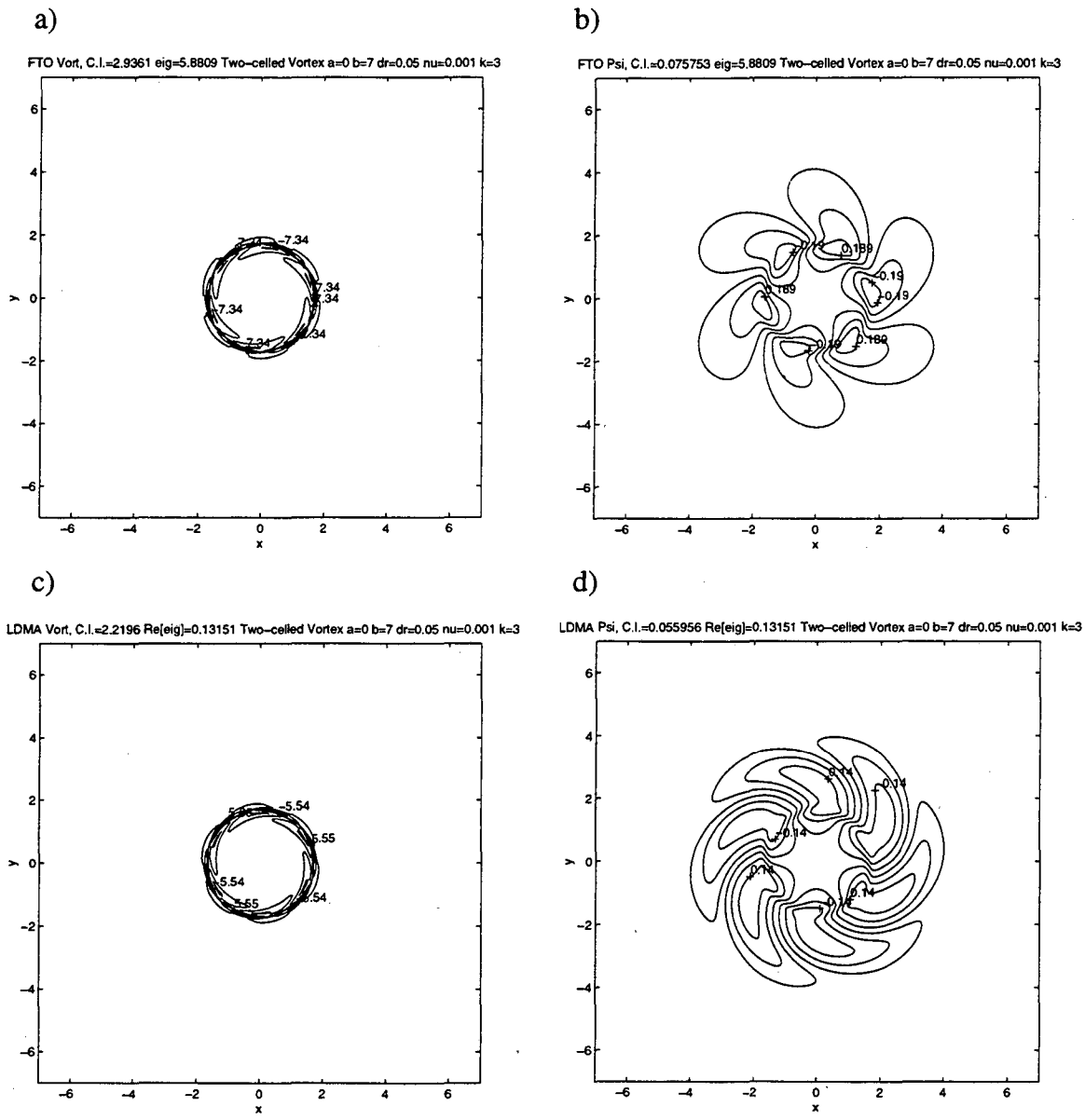

Figure 18 Vorticity and streamfunction fields for the t=5 FTO and the LDMA for k=3 in the two-celled vortex: a) FTO vorticity; b) FTO streamfunction; c) LDMA vorticity; d) LDMA streamfunction.

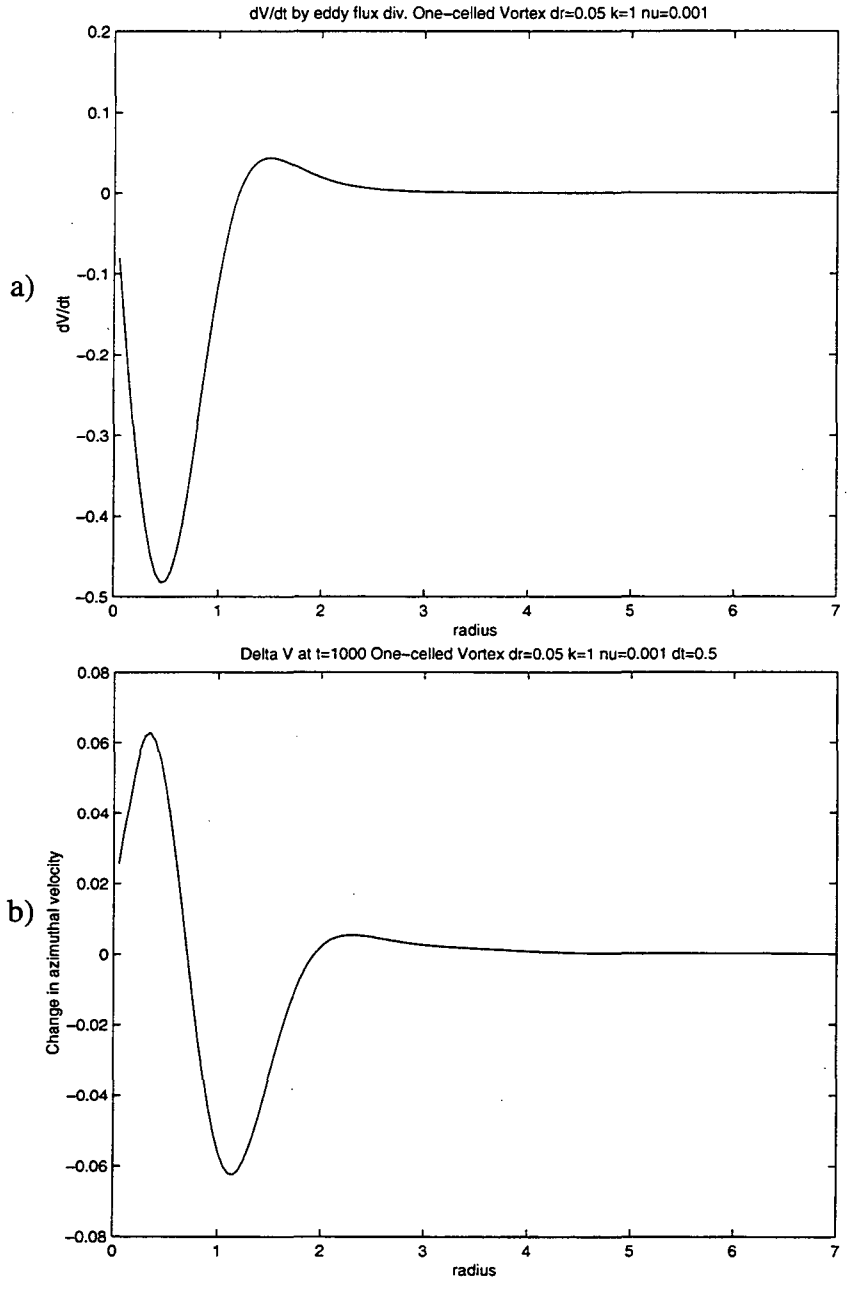

Figure 19 a) The instantaneous eddy momentum flux divergence of the k=1 IO in the one-celled vortex; b) The accumulated total momentum flux divergence from t=0 to t=1000 for the k=1 IO.

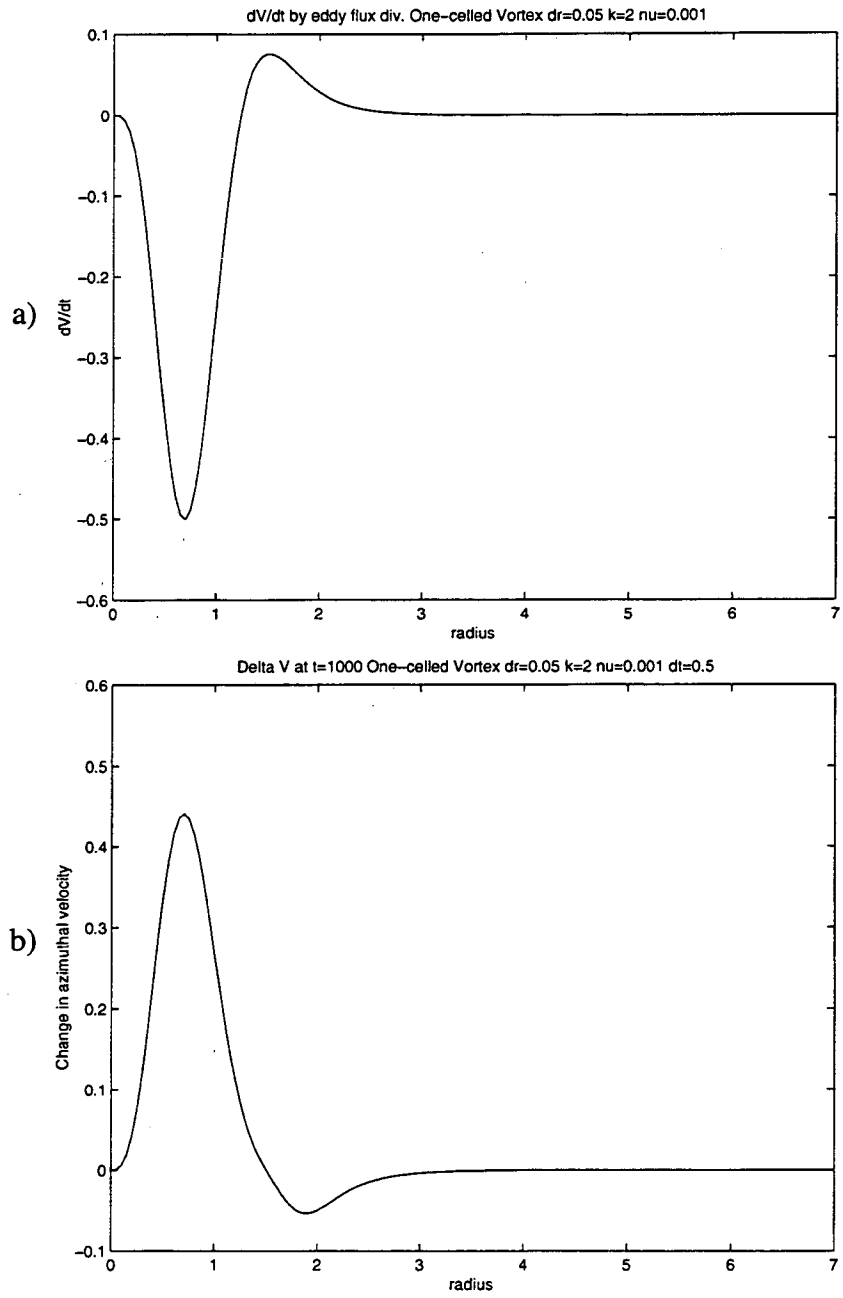

Figure 20 a) The instantaenous eddy momentum flux divergence of the k=2 IO in the one-celled vortex; b) The accumulated total momentum flux divergence from t=0 to t=1000 for the k=2 IO.

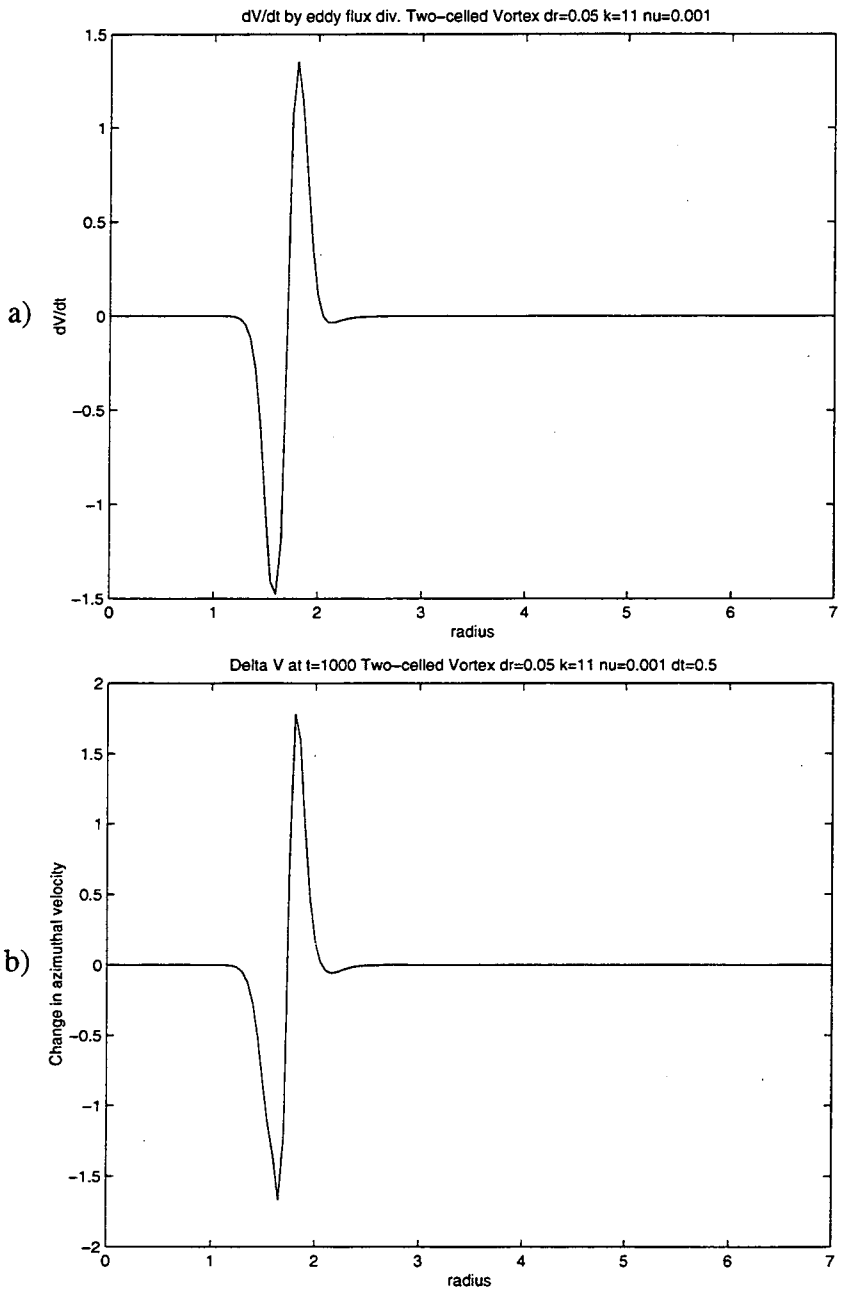

Figure 21 a) The instantaenous eddy momentum flux divergence of the complex conjugate of the k=11 IO in the two-celled vortex; b) The accumulated total momentum flux divergence from t=0 to t=1000.

a)

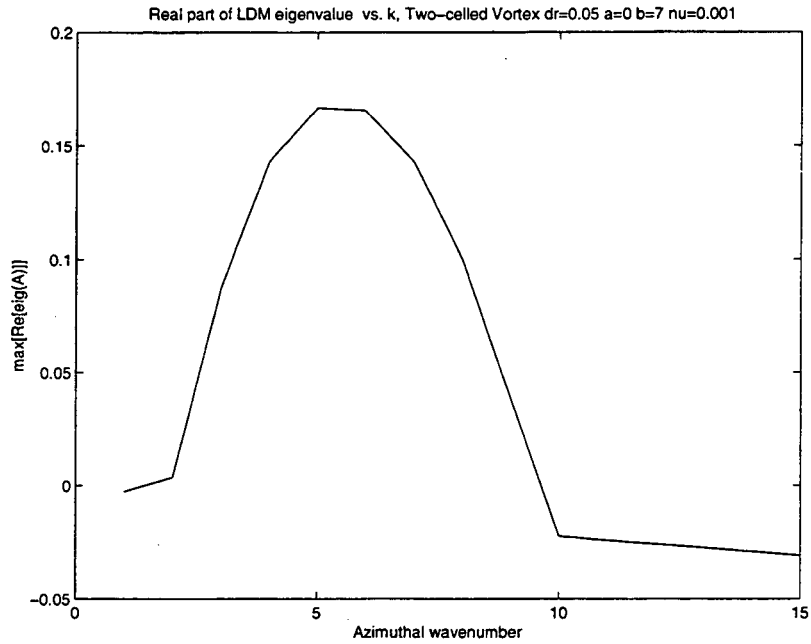

b)

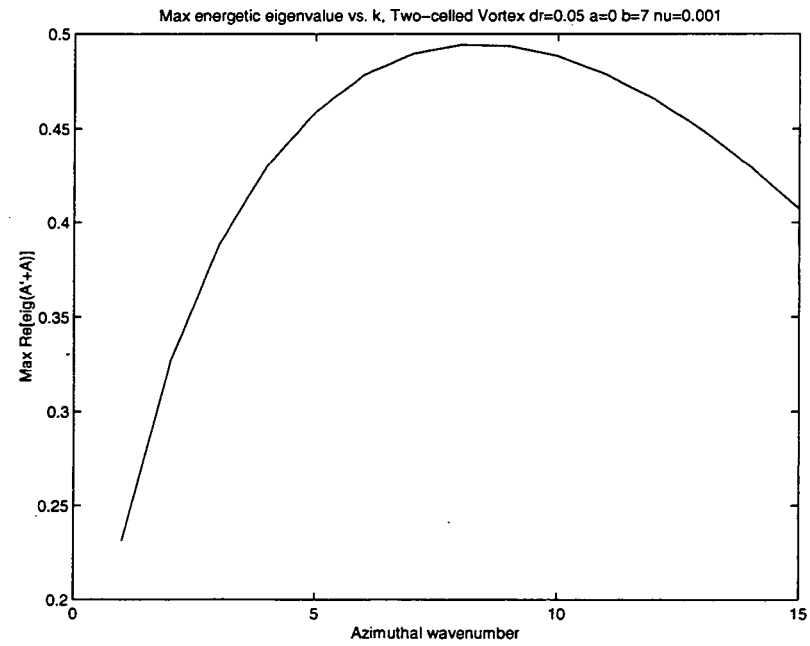

Figure 22 a) Real parts of the eigenvalues of the LDMs in the two-celled vortex and b) maximum instantaneous growth rates in energy in the two-celled vortex, when the stretching term has been removed from the vorticity evolution equation.

a)

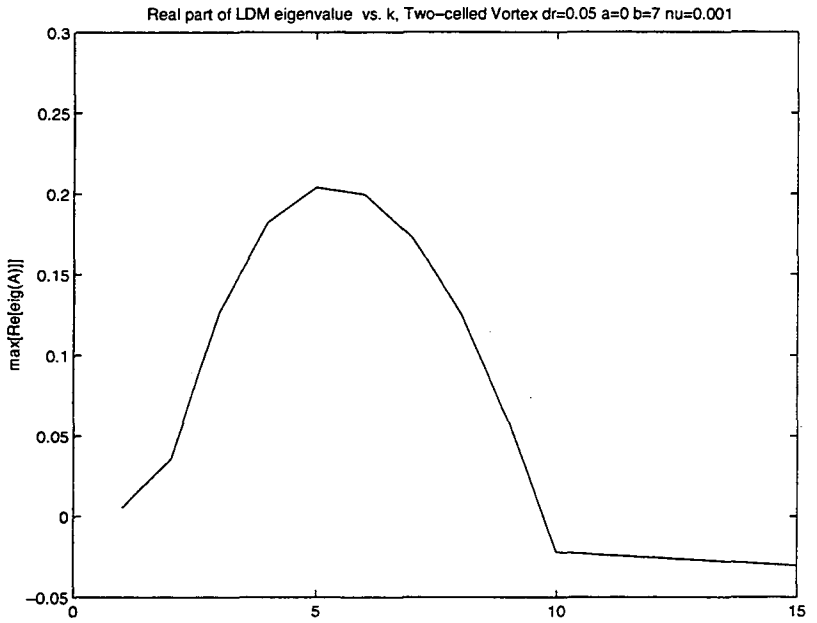

b)

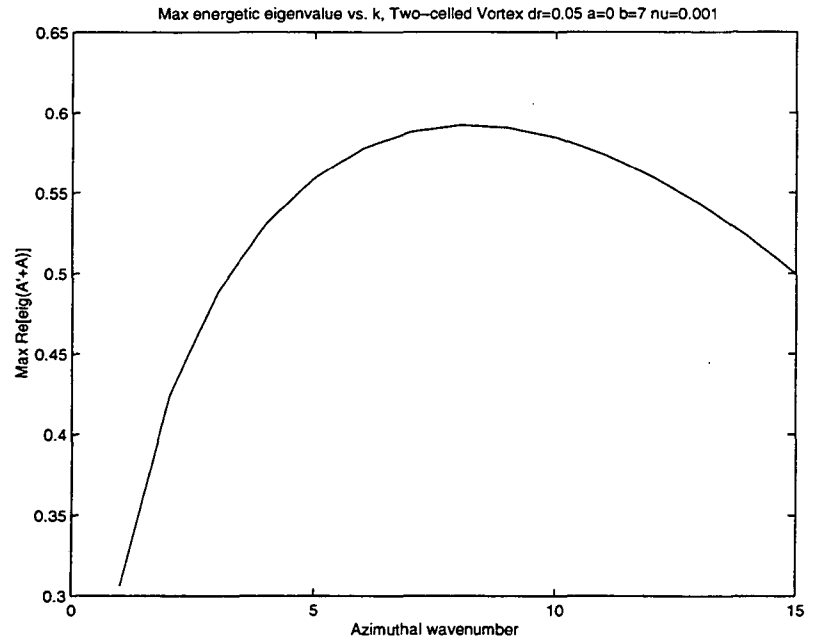

Figure 23 a) Real parts of the eigenvalues of the LDMs in the two-celled vortex and b) maximum instantaneous growth rates in energy in the two-celled vortex, when all terms associated with the radial inflow have been removed from the vorticity evolution equation.

a)

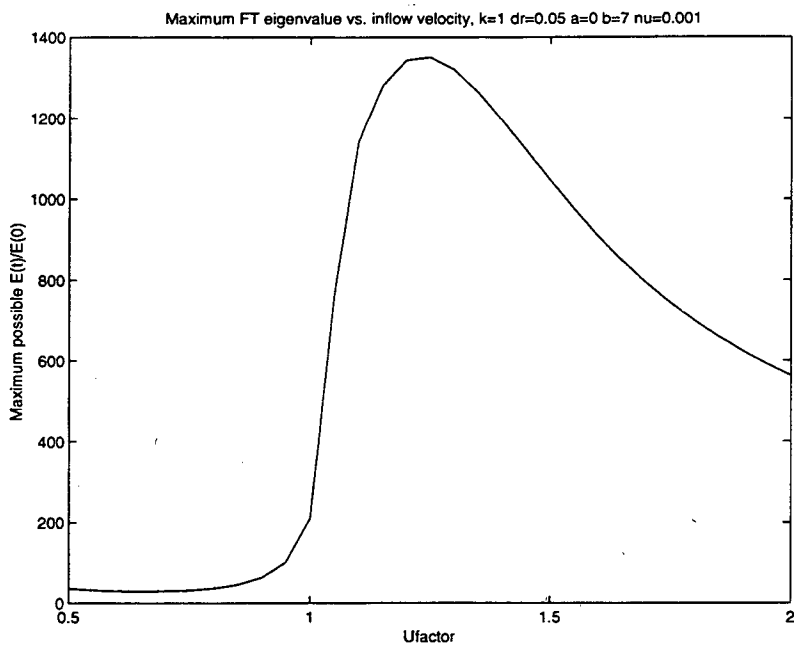

b)

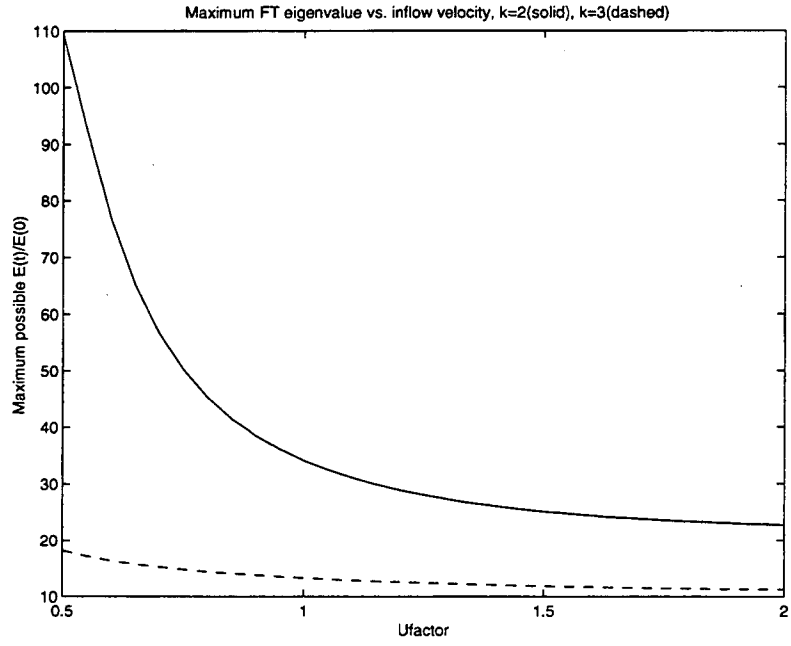

Figure 24 Maximum transient growth in the one-celled vortex as a function of the relative strengths of the radial inflow velocity which maintains the vortex: a) for azimuthal wavenumber k=1; b) for k=2 (solid) and k=3 (dashed).

a)

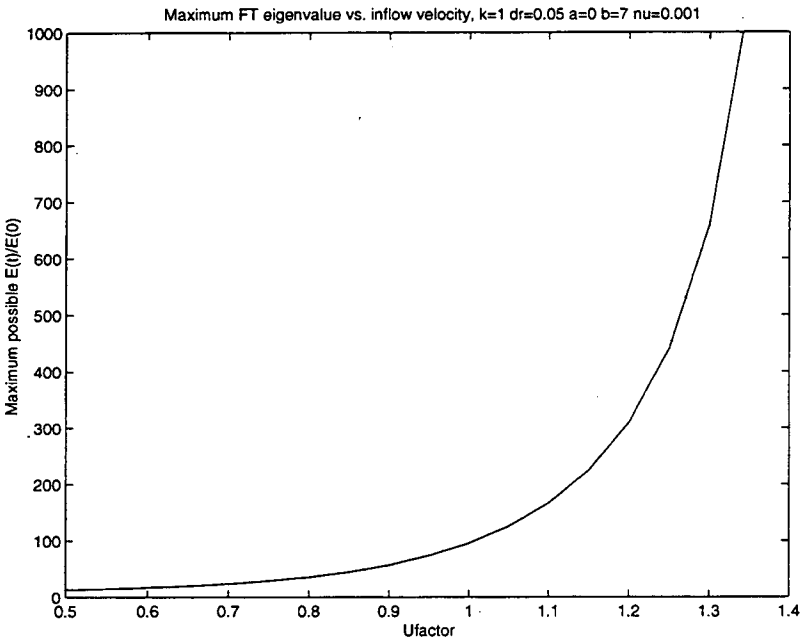

b)

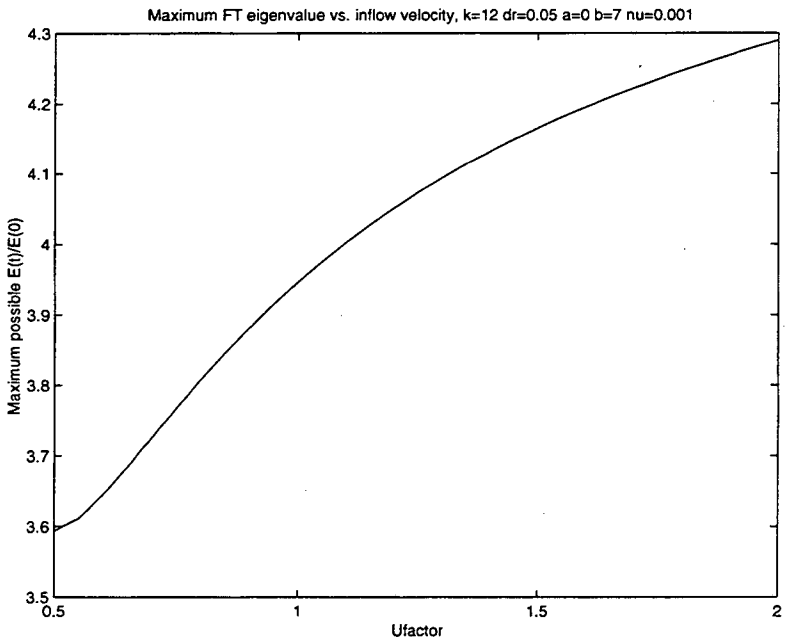

Figure 25 Maximum transient growth in the two-celled vortex as a function of the relative strengths of the radial inflow velocity which maintains the vortex: a) for azimuthal wavenumber k=1; b) for k=12. Note the domains are different in the two cases.

Ernest Orlando Lawrence Berkeley National Laboratory
One Cyclotron Road | Berkeley, California 94720

Prepared for the U.S. Department of Energy under Contract No. DE-AC03-76SF00098